DEGREE FINAL PROJECT MODEL A

Optimization of immunoprecipitation of Yap/Taz proteins from MLE12 immortalized murine lung epithelial cells

Inés Mínguez Santos

Biomedicine

Academic course 2021/2022

Experimental Sciences Faculty, Francisco de Vitoria University, Madrid, Spain

Supervisor: PhD. Renata K. Da Palma

Lung Bioengineering and Regeneration Laboratory, Lund University, Sweden

Supervisors: Hani N. Alsafadi and PhD. Darcy E. Wagner

ABSTRACT

Idiopathic pulmonary fibrosis (IPF) is a lethal lung disease characterized by repetitive injury resulting in scarring of mainly the distal lung epithelium. Hippo signaling pathway controls various homeostatic processes such as differentiation, proliferation, and migration. Its main effectors, Yap/Taz (Y/T), are dysregulated in IPF. Y/T are co-transcription factors that exert their target gene expression through binding to other transcription factors (TFs). The exact binding partners of Y/T are not known in IPF context. To address this, we have identified exact Y/T target gene motif sequences and subsequently inferred TFs associated with Y/T through bioinformatics tools. Our approach is to validate these TFs by mass spectrometry (MS) on pulled-down Y/T complexes in the subcellular compartments of lung epithelial cells. Thus, this project aims to optimize the immunoprecipitation (IP) protocol.

MLE12 cells were fractionated into cytoplasmic and nuclear compartments using MS-compatible buffers. IP optimization was done on MLE12 full lysates and subcellular fractions. The optimization included the addition of a preclearing step and variations in temperature and elution buffers from beads. Silver staining, western blotting (WB), and immunofluorescence were used to evaluate the results of optimization experiments.

We found that protein A magnetic beads showed less unspecific binding compared to protein G beads in WB. Moreover, protein A has a higher affinity for the antibodies of interest. Pull down was carried out using Y/T and IgG control antibodies. Additionally, proteins were eluted with low pH conditions followed by neutralization of the samples. Immunofluorescence of the beads after elution confirmed protein desorption, as well as silver staining after SDS-PAGE on these samples, showed bands corresponding to the complexes of interest in Y/T pull-down.

In conclusion, we have shown that protein A magnetic beads are suitable for the IP, and Y/T complexes are collected from the beads after low pH elution while retaining their compatibility with MS. This optimization enables the analysis of Y/T binding TFs through MS proteomics, which could be beneficial for the identification of pathological Y/T-TF interactions and their definition as new therapeutic targets while maintaining those that lead to pro-regenerative processes.

Keywords: Yap, Taz, immunoprecipitation, MLE12, idiopathic pulmonary fibrosis.

ACKNOWLEDGMENTS

Thank you to Darcy E. Wagner for hosting me in her research lab and for her support throughout my stay. Special thanks to Hani N. Alsafadi for supervising my project and teaching me with patience and 24-hour availability and Renata Kelly da Palma for her accompaniment from Spain.

I would also like to thank the whole group for creating a wonderful working environment and giving me feedback to help me improve as a scientist.

Thanks to María Ferrer for being the best partner I could have had in this amazing experience.

Finally, thank you very much to Lund University and UFV for giving me the opportunity to develop this project and improve my professional career.

ABBREVIATIONS

AEC1s: Alveolar epithelial type 1 cells

AEC2s: Alveolar epithelial type 2 cells

ATI: Alveolar type 1 cells

ATII: Alveolar type 2 cells

CUT&RUN: Cleavage under targets and release using nuclease

DMEM: Dulbecco's Modified Eagle Medium

ECM: Extracellular matrix

FB: Fractionation buffer

FBS: Fetal bovine serum

GPCRs: G-protein-coupled receptors

IP: Immunoprecipitation

IPF: Idiopathic pulmonary fibrosis

LATS1/2: Large tumor suppressor 1/2

MC: Mass spectrometry compatible buffer

MOB1A/B: MOB kinase activator 1A/B

MS: Mass spectrometry

MST1/2: Mammalian sterile 20-like kinases 1 and 2

MUC5B: mucin 5B, oligomeric mucus/gel-forming

ON: Overnight

PBS: Phosphate buffered saline

P/S: Penicillin and streptomycin

RT: Room temperature

SAV1: Salvador family WW domain-containing protein 1

TAZ: Transcriptional coactivator with a PDZ-binding domain

TEAD: Transcriptional enhanced associate domain

TFs: Transcription factors

TGF-β: Transforming growth factor beta

UIP: Usual interstitial pneumonia

WB: Western blotting

YAP: Yes-associated protein

Y/T: YAP and TAZ

INDEX

1. INTRODUCTION

1.1 Idiopathic pulmonary fibrosis

Idiopathic pulmonary fibrosis (IPF) is a chronic and progressive disease with unknown etiology that mainly affects the distal part of the lungs (1–3). It is a fibrosing disorder characterized by lung scarring and a specific histopathological pattern referred to as usual interstitial pneumonia (UIP). UIP is usually presented as alveolar fibrosis, bronchiectasis, and a characteristic radiological pattern known as honeycombing, which consists of small cystic airspaces randomly distributed and surrounded by fibrous tissue. Although there are other pathologies showing this pattern in high-resolution computed tomography, IPF can be distinguished by other laboratory and clinical features such as histopathology, the response to therapy and the natural history of the disease.

This disorder consists of the deposition of an excess of extracellular matrix (ECM) that leads to the scarring of alveolar tissue. As a result, the alveolar septa thicken preventing normal gas exchange, which causes symptoms such as dry cough, dyspnoea, and cyanosis in late stages (**Figure 1**). This normally ends with respiratory failure and death within 2-5 years of diagnosis due to the lack of effective therapies (3).

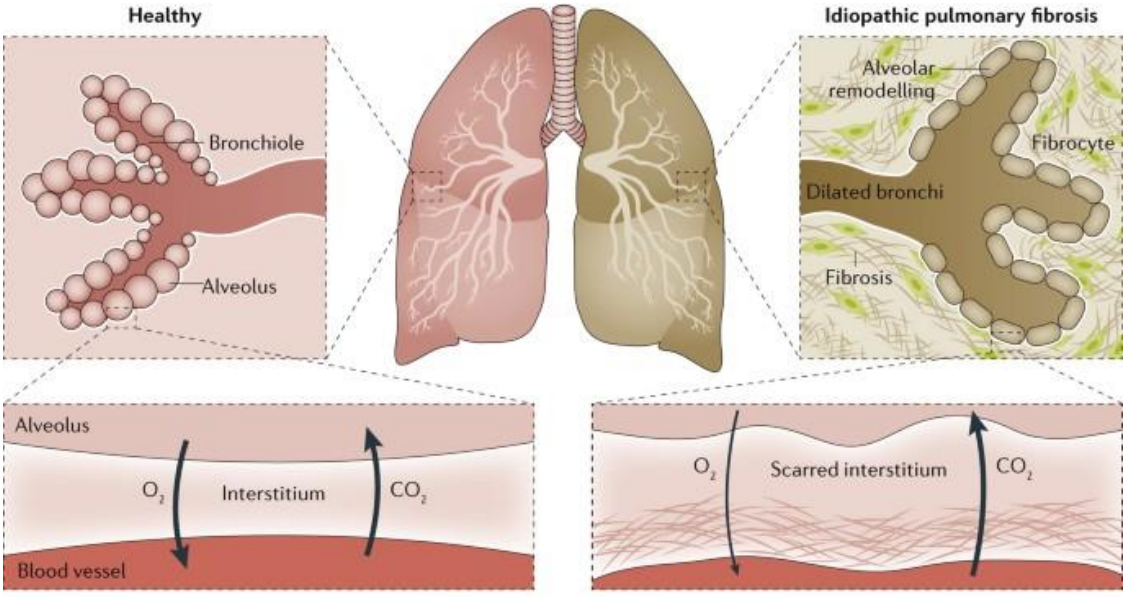

Figure 1. **Alveolar damage in idiopathic pulmonary fibrosis**. The disease causes bronchiectasis, alveolar remodeling, and an excess of extracellular matrix deposition, which hinders oxygen diffusion (3).

Several therapies have been tested without success, for example, anti-inflammatories have barely shown effectiveness, evidencing that inflammation plays a secondary role in the pathology. On the other hand, anti-fibrotic drugs such as nintedanib and pirfenidone have been approved for improving patient prognosis in some clinical trials. However, available therapies can only delay the development of the disease, hence IPF patients often resort to transplantation in a desperate attempt to survive. Therefore, an effective treatment is urgently needed (2–4).

1.2 Epidemiology and risk factors

More than 3 million people suffer from IPF worldwide. The incidence of this disorder differs in different parts of the world. Whereas in South America and East Asia the incidence is minimal with less than 4 cases per 100,000 people/year, in North America and Europe it is as high as 9 cases per 100,000 people/year (5). Prevalence is higher in men compared to women and is rated from 13 to 20 cases per 100.000 people (6), although it increases considerably with age. In fact, in patients older than 65 years old it has been estimated at 400 per 100.000 (3).

While the exact cause of IPF remains unknown, this disease has been correlated with several risk factors. It rarely appears in patients younger than 55 years old, which suggests that age is one of the most important predisposing factors. Additionally, some people are genetically susceptible to this disorder due to mutations in telomerase (TERT), genes encoding components of surfactant, or mucin 5B oligomeric mucus/gel-forming (MUC5B) gene, which disrupts mucin production and leads to increased susceptibility to alveolar epithelial cell injury. Other proposed origins include environmental factors. For instance, individuals exposed to wood, metal, and stone dust have shown an increased incidence (3). Viral infections and chronic gastroesophageal reflux have also recently been proposed as elements that can contribute to the pathogenesis of the disease. Interestingly, the most consistent behavioral risk factor among these is cigarette smoking. Therefore, it remains unclear whether the higher mortality and prevalence in men is a biological tendency or the result of behavioral factors (3–5).

1.3 Lung epithelium

The respiratory system can be divided into two different portions with different roles. The conducing portion includes the nose, pharynx, trachea, bronchi, and bronchioles and its

function is to filter, humidify and adjust the air temperature until reaching the respiratory portion, composed of air sacs named alveoli, where external respiration occurs (7,8).

Most of the respiratory tree is composed of pseudostratified columnar ciliated epithelium except for bronchioles, which transit to simple columnar and simple cuboidal epithelium when decreasing their caliber, and alveoli, that are revested by thin squamous epithelium to allow gas exchange (7). Several different cell types can be found in the lung epithelium. In the proximal region, the main ones are ciliated, non-ciliated secretory cells, and basal cells. With the branching of the respiratory tree and the subsequent change in epithelial type, Club cells, which are non-ciliated, become predominant, while alveoli are mainly formed by type I and II pneumocytes, also known as alveolar type I (ATI or AEC1s) and II (ATII or AEC2s) epithelial cells (7,9) (**Figure 2**).

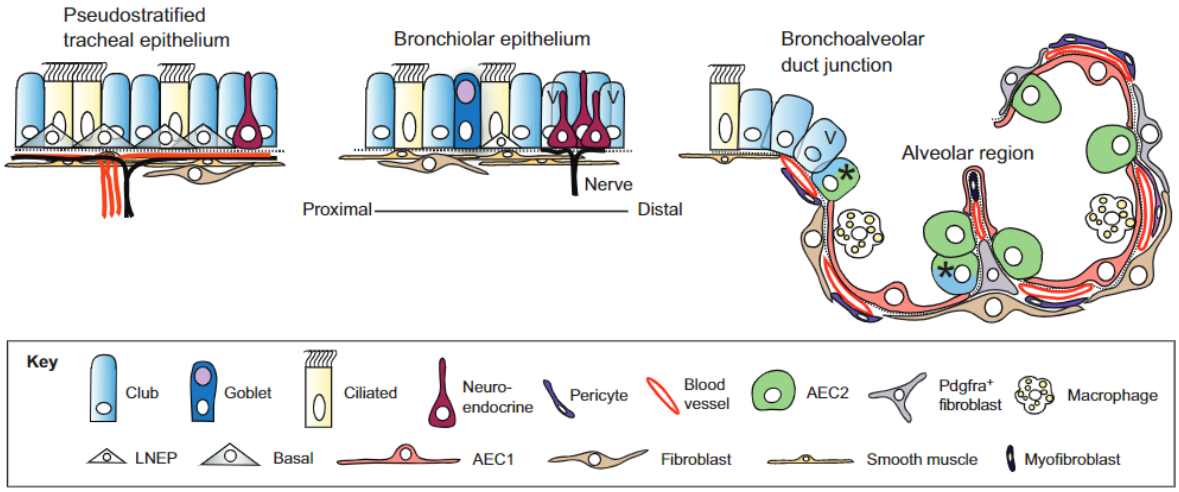

Figure 2. **Epithelial cell types of the mouse Lung**. The two major cell types that compose the alveolar region are type II (ATII) and type I (ATI) cells (9).

ATII cells produce and secrete surfactant protein C that prevents alveoli from collapsing during exhalation. They are considered the stem cells of the region due to their ability to self-renew and differentiate into ATI cells, acting as progenitors after injury in damaged alveoli. This is an extremely important role since ATI cells create the barrier that allows gas diffusion due to alveolar sacs are surrounded by blood capillaries, leaving a space in between, called the interstitium, that enables O_2 and CO_2 to diffuse through (7,10).

1.4 Pathophysiology

Lungs have the remarkable ability to repair the damage caused by injuries to which they are constantly exposed, but this capacity is limited and highly dependent on the type of injury. However, IPF results from the alteration in the re-epithelialization after repetitive alveolar epithelial cells micro-injuries (3,4).

When the lung is continuously exposed to harmful agents, pneumocytes are damaged and undergo apoptosis. In a healthy condition, ATII cells should regenerate normal lung alveolar epithelia but in IPF they demonstrate genomic instability, what makes them dysfunctional. On account of these cells do not produce surfactant protein C, mechanical tension increases, and epithelial cells depletion is exacerbated. All these events cause aberrant activation of neighboring epithelial cells that secrete profibrotic mediators such as transforming growth factor beta (TGF-β) that activate profibrotic pathways such as Smad signaling. When this pathway is triggered, it promotes fibrogenesis through the proliferation of resident mesenchymal cells and their subsequent differentiation into fibroblasts and myofibroblasts, while suppressing the transdifferentiation of ATII into ATI and thus, impeding regeneration (3,4,10–13). Moreover, there is evidence that TGF- β is the main driver of fibrosis and plays an important role in the fibrotic response (15). The resultant fibroblastic foci uncontrollably produce massive amounts of extracellular matrix (ECM) components. Consequently, scarring of the tissue occurs and lung architecture is destroyed, impeding respiration due to oxygen is unable to diffuse adequately through the interstitial space. (3,4). However, the pathogenesis of this disease and mechanisms underlying fibrosis are complex and not fully understood (1). Nonetheless, other studies have determined that the reactivation of different pathways involved in embryonic lung development such as hippo signaling pathway suppose a link between IPF and abnormal epithelial cells behavior as well as ageing (16).

1.5 Hippo Pathway

Hippo pathway is a conserved signaling cascade that maintains tissue homeostasis through the control of cellular proliferation, differentiation, survival, and organ size regulation, which are essential processes in tissue development and regeneration. The main effectors of this signal route are yes-associated protein (YAP) and the transcriptional coactivator with a PDZ-binding domain (TAZ). Both are co-transcriptional factors, which means that they do not have their own DNA binding motifs, but rather require interaction with other proteins, mainly with transcriptional enhanced associate domain (TEAD) transcription factors (TFs), to induce gene expression (17). The fundamental difference between YAP and TAZ (Y/T) is that although both

contain WW domains to mediate protein-protein interactions, YAP contains two of them whereas TAZ has only one (18). In addition, they can bind to different TFs, but also present overlap as seen with TEAD transcription factors suggesting that they share redundancy in some biological contexts (15).

Hippo pathway responds to cellular microenvironmental stimuli including cell-cell contact, mechanical signals, cellular stress, or diverse soluble factors. As a response, upstream regulators can activate the signaling cascade by phosphorylation of mammalian sterile 20-like kinases 1 and 2 (MST1/2) serine-threonine kinases. MST 1/2 in combination with their activating adaptor protein Salvador family WW domain-containing protein 1 (SAV1) form an active enzyme complex that phosphorylates large tumor suppressor 1/2 (LATS1/2) kinases and MOB kinase activator 1A/B (MOB1A/B). In turn, Y/T are phosphorylated by activated LATS1/2. This phosphate group inactivates Y/T and allows the interaction with 14-3-3 proteins causing their cytoplasmic retention. However, phosphorylated Y/T can also be polyubiquitinated and subsequently degraded via proteasome. On the other hand, in the absence of Hippo kinase complex activation, Y/T can translocate to the nucleus and interact with TEAD TFs to induce the expression of multiple genes involved in proliferation, differentiation, and cell survival (17,19) (**Figure 3**).

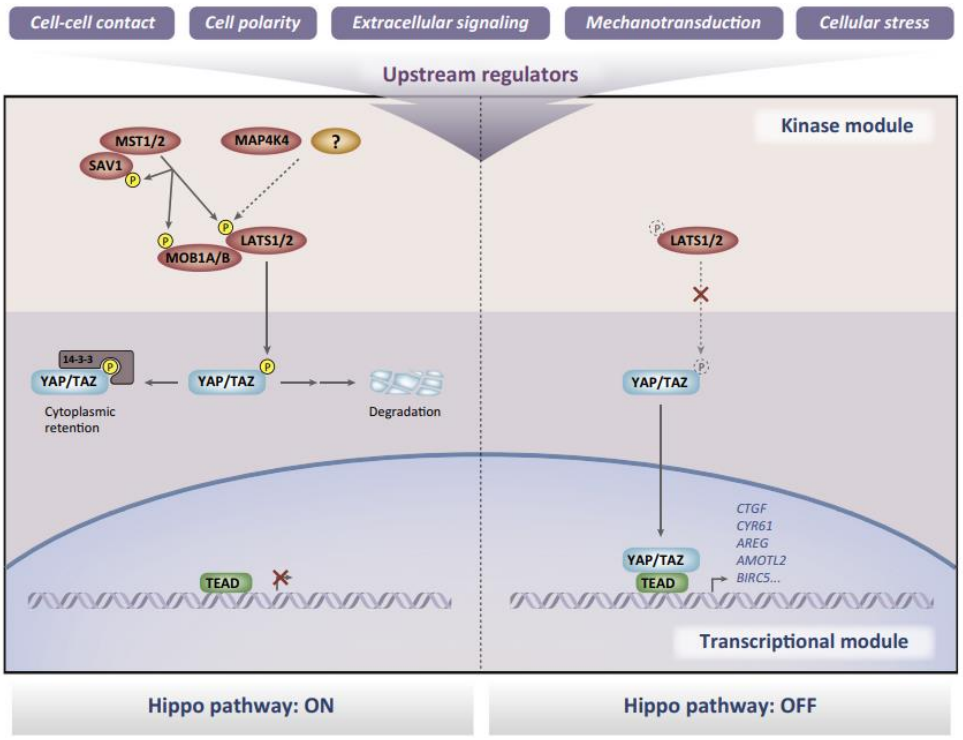

***Figura 3*. Hippo signaling pathway.** Microenvironmental stimuli regulate serine-threonine kinase module. Hippo pathway activation causes YAP/TAZ phosphorylation and retention in the cytoplasm. By contrast, when the kinase module is inactivated, YAP/TAZ can enter de nucleus inducing gene expression when interacting with transcription factors, prominently, TEA domain family members (17).

1.6 Upstream signals that regulate Hippo pathway

Y/T are the main effectors of the Hippo pathway. Their phosphorylation and consequent inactivation or translocation to the nucleus when activated, is a response to diverse stimuli that regulate the core kinase cascade. Some of them are physical cues, soluble factors, stress signals, or cell polarity. The upstream regulators can act on either of the kinases in the cascade.

Development and organ growth involve cell processes to adapt to extracellular mechanical cues. In fact, tissue architecture can physically restrict cell growth and proliferation. For example, high cell density promotes inhibitory signals to stop proliferation in which Hippo pathway is involved. As a result of cell-cell contact, adherens and tight junctions are increased in confluent cells, which induce activation of LATS 1/2 and inactivation of Y/T. Moreover, cell attachment, which is essential for them to survive, and ECM stiffness also plays a role in the regulation of Y/T activities through changes in cell geometry and cytoskeleton tension. This provides mechanical signal inducing YAP nuclear localization through activation of Rho-GTPases or the FAK–Src–PI3K pathway, which inhibit LATS 1/2. Indeed, cells grown on stiff ECM are flat and show YAP in the nucleus while cells grown on soft ECM, on a small surface, or detached from a culture plate are round and show cytoplasmic retention of YAP (20–22).

Nutrients and hormones are also indispensable to maintain cells alive and let them grow. Furthermore, it has been speculated that extracellular molecules such as growth factors might regulate Hippo pathway to control homeostasis. G-protein-coupled receptors (GPCRs) are the largest and most diverse group of membrane receptors, and they regulate Hippo pathway as a response to hormonal cues. Nevertheless, depending on the nature of downstream G proteins, GPCRs can either activate or inhibit the LATS kinase to stimulate or inhibit YAP activity. For example, Gα12/13- and Gαq/11-coupled GPCRs activate Rho-GTPases which inactivate LATS 1/2. In contrast, active GαS-coupled GPCRs induce LATS kinases activation which in turn suppresses YAP activity (17,20). In addition, other ligands such as Wnt proteins can activate Y/T through Gα12/13 coupled GPCRs. This shows an evident crosstalk between both pathways. In fact, it has been demonstrated that Wnt, TGF-β, and Hippo pathway converge into a complex network which governs activation and maintenance of myofibroblasts, who produce the typical fibrotic phenotype characterized by excessive synthesis, remodeling, and contraction of extracellular matrix (15,20).

1.7 Hippo pathway in IPF

Mechanical properties of Y/T have been related to the induction of fibrosis through myofibroblasts activation. Moreover, Y/T show increased nuclear localization and elevated protein levels in IPF biopsies, suggesting an incremented transcriptional activity (23)(15). In addition, recent studies from Darcy Wagner´s group have shown that Y/T proteins play an important role not only in (myo)fibroblasts but also in epithelial cells in the context of fibrosis. These proteins' expression was found to be increased in alveolar cells indicating that they contribute to the modulation of fibrotic changes (unpublished data). Moreover, targeting Y/T activity in the fibrotic mouse model using a pharmaceutical drug (Verteporfin) showed amelioration of the fibrotic phenotype and improved survival in vivo (unpublished data). However, while verteporfin was found to decrease the fibrotic phenotype in mice, it did not manage to recover epithelial loss. This indicates that Verteporfin inhibits all Y/T activity regardless of whether it is pro-fibrotic or pro-regenerative. The exact function of Y/T and the exact transcription factors that they bound to in the fibrotic condition in lung epithelial cells remain unclear. Thus, further research is needed to elucidate which are the transcriptional complexes containing Y/T and identify possible differences between healthy and fibrotic lung epithelium. The importance of understanding the exact function of these proteins in the fibrotic context lies in the fact that Y/T are involved in regenerative processes necessary for lung tissue restoration. Therefore, identification of which interactions promote the pro-fibrotic condition will allow targeting disease-causing associations while keeping intact those that drive regenerative processes.

To address this, cleavage under targets and release using nuclease (CUT&RUN) technique was performed in several mouse lung epithelial cell types to identify the exact target gene motifs that are activated. CUT&RUN is based on chromatin immunoprecipitation and consists of targeting Y/T with an antibody bound to magnetic beads. Then, a bacterial nuclease cuts DNA around TFs binding site to immunoprecipitate those complexes and finally sequence DNA after its release. Subsequently, bioinformatics tools were used to predict several transcription factors that could be associated with Y/T. However, this information needs to be verified. Validation will be performed through subcellular fractionation of lung epithelial cells followed by immunoprecipitation (IP) and mass spectrometry (MS) analysis. Nevertheless, the IP protocol needs to be optimized to be compatible with MS.

In this study, we have validated the MS compatible subcellular fractionation protocol in mouse lung epithelial cells (MLE12 cell line) as well as examined the effect of TGF-β treatment on these cells. Nevertheless, alternative nuclear markers need to be explored to confirm

successful fractionation in TGF- β-treated samples. Additionally, we optimized an IP protocol to purify Y/T protein complexes from MLE12 lysates suitable for MS proteomics analysis. The IP was performed using protein A magnetic beads and low pH elution buffers followed by the appropriate neutralization.

2. OBJECTIVES

The overall aim of this project is the optimization of an immunoprecipitation protocol to pull down Y/T complexes from mouse lung epithelial cells, so that binding TFs can be identified through mass spectrometry proteomics.

To this end, the following specific objectives were established:

1. Validate subcellular fractionation protocol in MLE12 cells maintaining mass spectrometry proteomics compatibility.
2. Analyze suitability of protein A magnetic beads for Y/T pull down.
3. Determine the appropriate concentration of antibodies to immunoprecipitate Y/T proteins.
4. Test various mass spectrometry compatible elution buffers to separate pulled down proteins from the magnetic beads.

3. MATERIALS AND METHODS

3.1 Reagents

Reagent	Company	Product number	Notes
DMEM/F12 medium	Gibco™	#11320033	supplemented with 10% fetal bovine serum (FBS), 1% penicillin/streptomycin (P/S) (10.000 U/ml)
Fetal bovine serum (FBS)	Gibco™	#10270106	-
Penicillin/Streptomycin (P/S)	Gibco™	#15140122	10.000 U/ml
Phosphate buffered saline 1X (PBS)	HyClone™	#SH30256.01	-
Trypsin protease	HyClone™	#SH30236.01	Trypsin 0.05% protease solution
TrypLE Express	Gibco™	#12605010	-
PureCol® Type I Collagen Solution	Advanced BioMatrix	#5005	3 mg/ml (Bovine)
BCA protein assay Kit	Thermo Scientific™	#10209523	Reducing agent compatible
ROTIblock	Carl Roth	#A151.1	-
ECL substrate	Bio-Rad	#1705061	-
Triton™ X-100	Sigma-Aldrich	#T9284-500ML	-
Tris-buffered saline	Thermo Fisher	#28360	TBS
HEPES	MP Biomedicals	#1688449	-
KCl	Scharlau	#PO02001000	-
$MgCl_2$	Acros organics	#197530010	-

EDTA	Duchefa Biochemie	#E0511.0500	-
EGTA	VWR International	#0732	-
NP-40	EMD millipore	#492016	-
Glycerol	Honeywell	#15523-1L	-
Protease inhibitor	Sigma-Aldrich	#4693132001	1 pill per 10 mL buffer
Phosphatase inhibitor	Sigma-Aldrich	#4906837001	1 pill per 10 mL buffer
NaCl	Fisher Scientific	#11328544	-
$Na_4P_2O_7$	Sigma-Aldrich	#P8010	-
Sodium deoxycholate	Sigma-Aldrich	#30970	-
Tris	Saveen & Werner	#T1000-5	-
HCl 6.0N solution	Fisher Scientific	#15402077	-
40% acrylamide	Roth	#T802.1	(37,5:1)
SDS	VWR International	#A7249.0500	-
APS	Fisher Scientific	#10266400	-
TEMED	Sigma-Aldrich	#T9281	-
2,2,2 trichloroethanol	Sigma-Aldrich	#T54801	-
Bromophenol blue	VWR International	#0312-50G	-
2-propanol	Fisher Scientific	#603117000	-
Methanol	VWR International	# 20837320	-
Tween-20	VWR International	# 28829296	-
TGF-β	R&D Systems	#7666-MB-005/CF	Working solution at 10ng/mL
IgG Elution buffer	Fisher Scientific	#21028	pH 2.0
Citric acid	Fisher Scientific	#10655102	-
Guanidine	Sigma-Aldrich	#G9284	-
Glycine	Millipore Sigma	#G8898-1KG	-
Acetic acid	Fisher Scientific	# 10304980	-

3.2 Antibodies

Company	Antibody	Product number
Cell Signaling Technology	Phospho-SMAD2 (Ser465/467) rabbit monoclonal antibody	#138D4
	Smad2/3 antibody Sampler Kit	#12747
	YAP/TAZ Rabbit monoclonal antibody	#D24E4
	phospho-YAP (Ser127) rabbit monoclonal antibody	#D9W2I
	GAPDH (14C10) rabbit antibody HRP Conjugate	#3683
Abcam	Anti-TAZ antibody	#ab84927
	Anti-lamin B1 antibody	#ab16048
	Recombinant Rabbit IgG isotype control	#ab172730
Invitrogen	IgG (H+L) highly cross-adsorbed donkey anti-Rabbit HRP polyclonal antibody	#A16035
	IgG (H+L) Cross-Adsorbed Goat anti-Rabbit conjugated with Alexa Fluor 568	#A11011
	Rabbit IgG Isotype Control	# SP137

3.3 Buffers preparation

Fractionation buffer (FB)	Mass spectrometry compatible buffer (MC)	RIPA buffer
25mM HEPES, 5mM KCl, 25mM MgCl2, 0,05mM EDTA (pH=7), 0,1% NP-40, 10% glycerol.	25mM Tris-HCl (pH=7,5), 300mM NaCl, 1mM EDTA (pH=7). **Adjust pH to 7-8**	20 mM Tris-HCl pH 7.4, 150 mM NaCl, 1 mM EDTA, 1 mM EGTA, 1% NP-40, 1% sodium deoxycholate, 2,5 mM Na4P2O7
+ Protease & phosphatase inhibitors. (1 pill /10mL)		

3.4 Cell culture and maintenance

The murine lung epithelial cells MLE 12 (ATCC CRL-2110) were grown in Dulbecco's Modified Eagle Medium (DMEM/F12 medium) supplemented with 10% FBS and 1% penicillin/streptomycin (10.000 U/ml). Cells were cultured in T-75 flasks and incubated in a humidified atmosphere with 95% air and 5% of carbon dioxide at 37ºC. The media was changed every 2 days and cells were split when they reached 85-90% of confluence.

To split the cells, warm phosphate-buffered saline (1X PBS) was first used to wash and remove α1-antitrypsin present in FBS, then cells were dissociated with trypsin 0.05% protease solution or TrypLE previously warmed. Trypsinization was performed at 37ºC for 5 minutes and subsequently stopped by the addition of DMEM/F12. Finally, cells were counted and sewed at a concentration of 50.000 cells/mL.

3.5 TGF-β treatment

Cells were plated in petri dishes (Sarstedt #82.1473.001) at a concentration of 50.000 cells/mL (10 mL/plate) until confluency. 10 hours of starvation was applied using DMEM/F12 supplemented with 1%P/S without FBS after 3 washes with warm PBS. Once the starvation time finished, 10 ng/mL TGF-β treatment was applied for 4 hours. Finally, cells were trypsinized, washed with PBS, and frozen to stop the treatment.

3.6 Protein extraction

Cells were grown in petri dishes or 6 well plates both previously coated with collagen type I. Some of them were subjected to subcellular fractionation while other ones were fully lysed.

- For **subcellular fractionation**: Cytoplasmic fraction of the samples was obtained by treating with FB and incubating for 20 minutes on ice, for adherent cells it was necessary to scratch the surface of petri dishes. Each sample was then triturated with a 27gx3/4 hydraulic needle six times and centrifuged at 4ºC 1000xg for 10 minutes. The resultant supernatant contained the cytoplasmic fraction.

  For the extraction of the nuclear fraction, the pellet obtained was washed with FB and spun down for 10 minutes, 1000xg at 4ºC twice for later resuspend the pellet in MC and incubate it for 10 minutes on ice. 3-5 minutes of sonication was applied, and samples were centrifuged at maximal speed (16602 x g) for 20 minutes at 4ºC using Centrifuge Sigma 1-14K (Sigma #10020). The resultant supernatant contained the nuclear fraction (**Figure 4**).

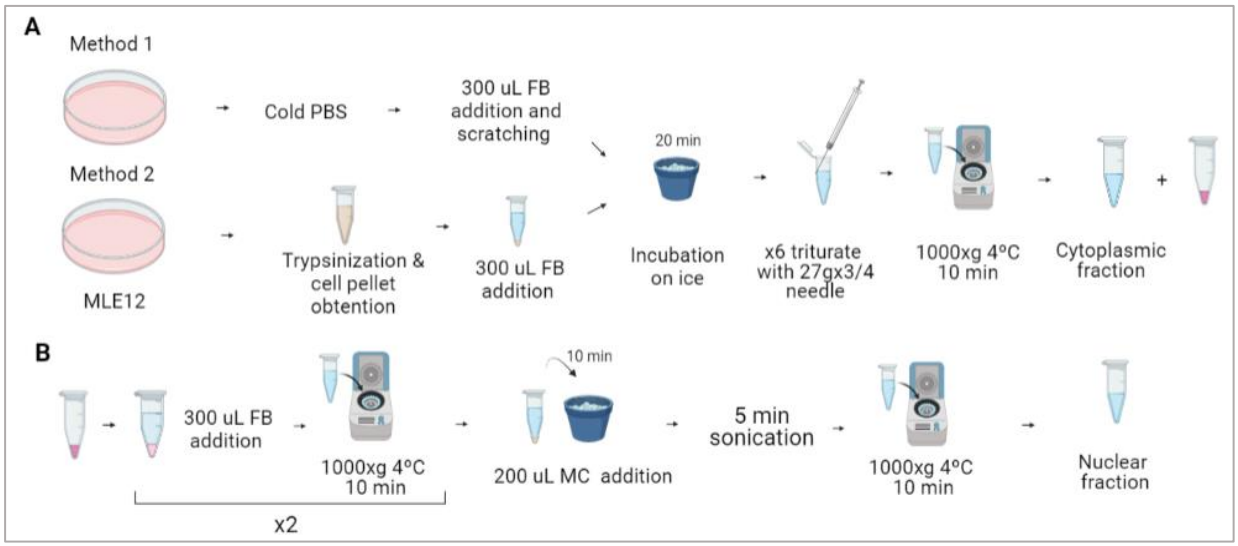

Figure 4. **Schematic of subcellular fractionation protocol.** A) Cytoplasmic fraction obtention. Method 1 corresponds to adherent cells while method 2 is applied to obtain cells in suspension before fractionation. B) Nuclear fraction obtention. FB= fractionation buffer MC= mass spectrometry compatible buffer. Created with Biorender.

- For **full lysates**: Adherent cells were treated with cold PBS, then 300 µL of RIPA buffer were added to scrape the surface of petri dishes while in the suspension condition cells were trypsinized and washed with PBS before adding 300 µL of RIPA to the pellets. After an incubation of 15 minutes on ice, all samples were centrifuged at the highest speed 15 minutes at 4ºC. The resultant supernatant contained cell proteins.

3.7 Immunoassays

- **Western blotting**: Protein quantification was performed with BCA assay using the appropriate buffer (RIPA, FB, or MC) to do standard curves and the absorbance was measured by Epoch microplate spectrophotometer (BioTek) at wavelength(λ) 562nm. Once samples were mixed with reducing loading buffer containing β-mercaptoethanol and boiled at 95ºC for 5 minutes, SDS-PAGE was performed using stain-free tris-HCl 1,5mm 10% homemade gels (**Table S1**). After wet transfer (250 mA for 90 min), the polyvinylidene fluoride membrane was blocked with ROTIblock and then incubated with antibodies for 1 hour at room temperature (RT) or 4ºC overnight (ON). Bound antibodies were detected after incubation with ECL substrate using a ChemiDoc imaging system (Azure c-600). ImageLab software v6.1.0 (Bio-Rad) was used to process blot images.

- **Immunofluorescence:** samples containing protein A magnetic beads before and after elution of rabbit specific antibodies (Y/T or IgG isotype control) were mixed with 100 µL of

cross-adsorbed goat anti-rabbit conjugated with Alexa Fluor 568 antibody solution (1:100 in wash buffer composed of tris-buffered saline containing 0,05% Tween-20 and 0,5M NaCl). After 30 minutes of incubation RT and 3 washes with wash buffer, samples were placed in a 96 well plate (Sarstedt # 83.3924) and imaged with Cytation 5 cell imaging multi-mode reader (Biotek) using 20X Bright Field and Texas Red channels (586,647). Images were processed using Fiji image J.

- **Immunoprecipitation:** protein A magnetic beads (Fisher Scientific # 13404229) were used to perform immunoprecipitation (IP) experiments. Firstly, samples were subjected to pre-clearing to reduce non-specific protein binding to the beads. To do this, magnetic beads were washed twice with the appropriate lysis buffer (FB, MC, or RIPA) and then incubated with the protein sample without adding antibodies for 20 minutes RT. The resultant beads were separated with a magnetic rack and discarded. Immunoprecipitation was performed in the pre-cleared lysates following the beads manufacturer protocol. Proteins were eluted using different condition buffers: IgG Elution buffer, SDS-PAGE reducing sample buffer, 100 mM glycine•HCl pH 2.5-3.0, 100 mM citric acid, pH 3.0, 0.1M glycine•NaOH pH 10.0, 3.0 M potassium chloride, 2-6 M guanidine•HCl and 1% sodium deoxycholate. The eluted samples were neutralized when needed and analyzed with silver staining using Pierce Silver Stain Kit (Thermo Scientific™ # 24612) or western blot after SDS-PAGE (**Figure 5**).

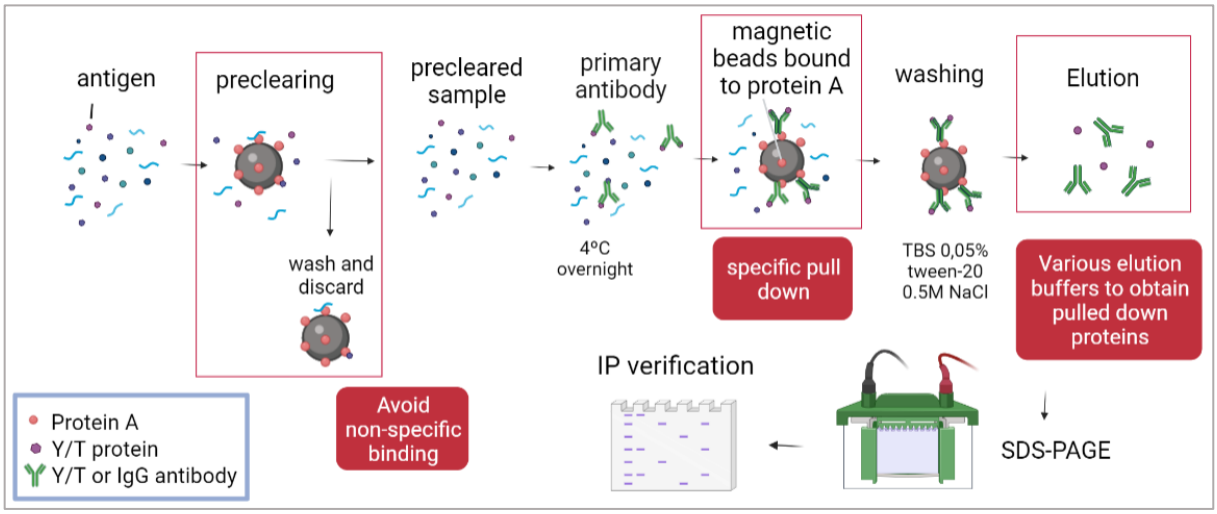

Figure 5. **Schematic of immunoprecipitation protocol with the addition of a preclearing step.** Precleared antigen sample is combined with the specific antibody and the volume is adjusted with the lysis buffer to 500 uL. The reaction is incubated at 4ºC over night with rotation. Protein A magnetic beads previously washed with wash buffer (TBS 0,05% tween-20 0,5M NaCl) are added to the sample/antibody mixture for 1 hour RT with mixing. Beads are collected using a magnet, washed twice with wash buffer and one time with ultrapure water. Finally, bound proteins are eluted using the appropriate buffer. The resultant samples are loaded in an SDS-PAGE to perform silver staining or western blotting. Picture created with Biorender.

4. RESULTS

For a better understanding of the results, it is important to comprehend the experimental approach. This overview is shown in **figure 6**.

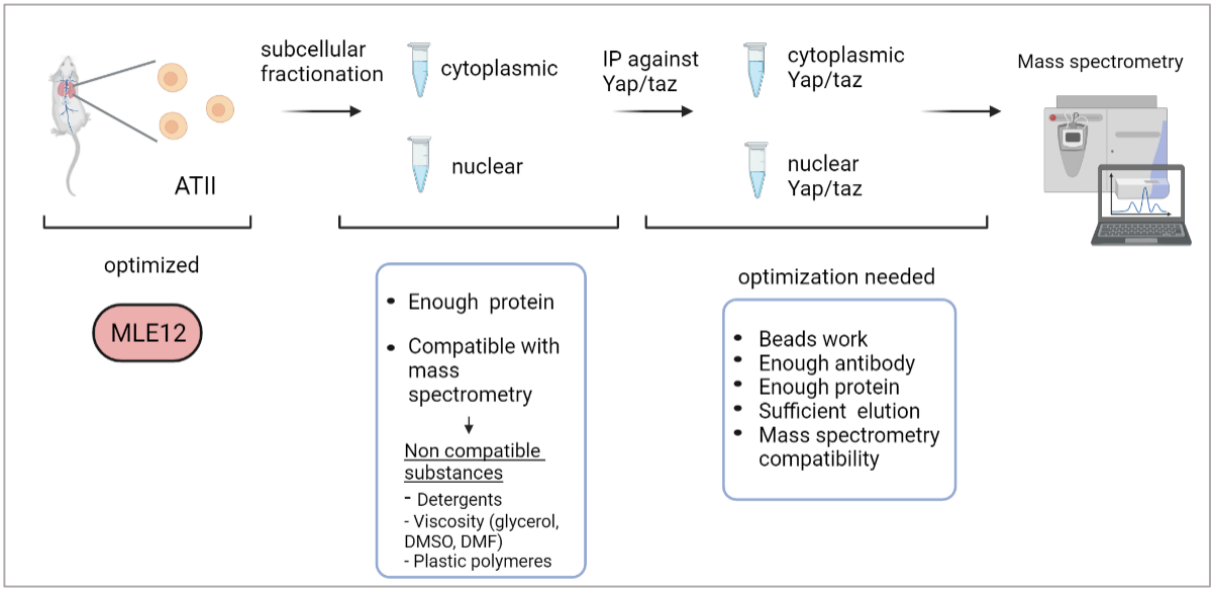

Figure 6. **Overview of the experimental process**. MLE12 cells are subcellular fractionated to separate the cytoplasmic and nuclear compartments. Subsequently, Y/T immunoprecipitation is performed to obtain the complexes formed by these proteins. Once the immunoprecipitation process is optimized and validated, proteins that interact with Y/T will be identified through mass spectrometry proteomics. Image created with Biorender.

4.1 Validation of the effectiveness of the subcellular fractionation protocol

4.1.1 Subcellular fractionation protocol separates cytoplasmic from the nuclear fraction in MLE12 cells

Optimization of molecular techniques requires large number of cells and several attempts which make it difficult to use primary cells for that purpose. Therefore, we used an immortalized cell line to do the optimization to avoid the usage of mice unecessarily. We used MLE12 cells as a model celltype for alveolar type II cells as their morphology resembles that of ATII cells. In order to faithfully recreate the biological context of mice to better understand the molecular mechanisms underlying the disease, we performed the experiments on MLE12 cells trypsinized or maintained adherent prior to subcellular fractionation, since ATII cells are in suspension when obtaining them from the animal.

There were no differences observed in the total amount of proteins between both suspended and adherent cells (**Figure 7A**) . However, the nuclear fraction obtained from the trypsinized cells was found to be considerably higher. Additionally, WB on these samples using well-known nuclear (Lamin B1) and cytoplasmic (GAPDH) markers shows completely differentiated bands in cytoplasmic and nuclear fractions of both adherent and suspended cells, demonstrating that the protocol satisfactorily separates proteins from the distinct compartments.

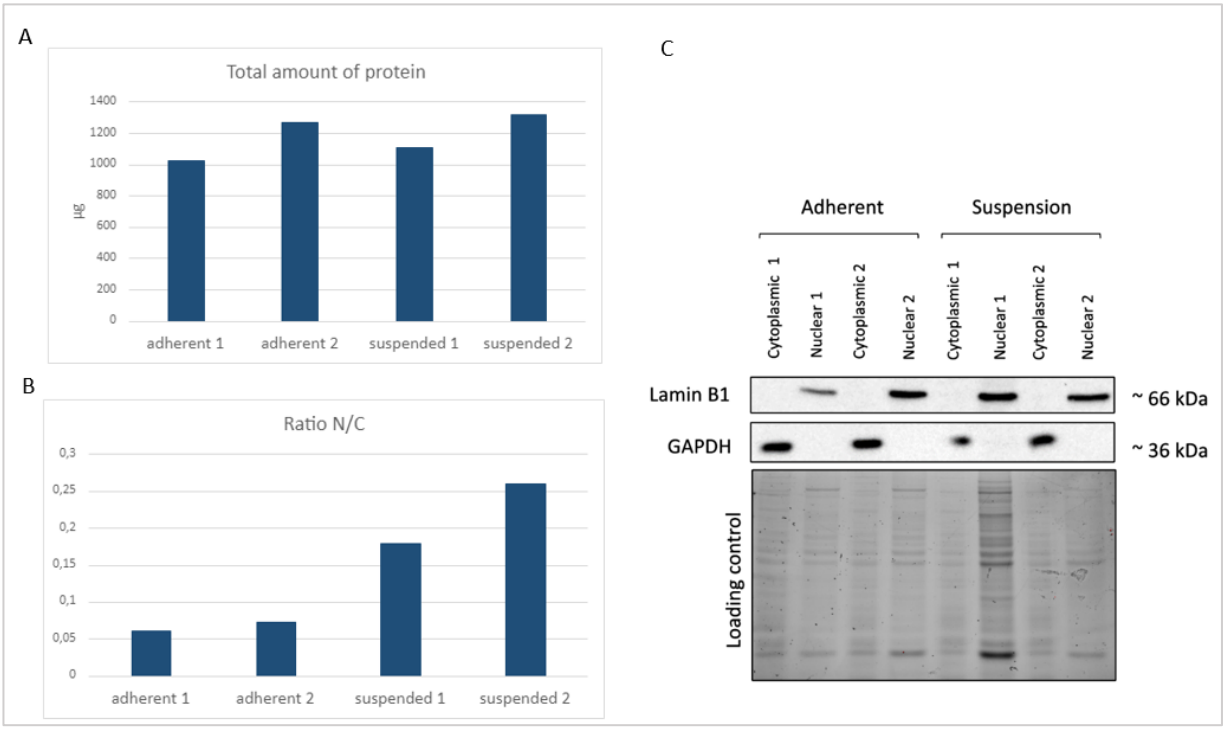

Figure 7. **Subcellular fractionation protocol separates effectively nuclear from cytoplasmic fraction in MLE12 cells.** (A) Total amount of proteins in µg obtained after subcellular fractionation from adherent and suspended cells measured with BCA assay at 562λ. (B) Nuclear to cytoplasmic fraction ratio in adherent trypsinized MLE12 cells. (C) Western blot analysis of adherent and suspended cells using Lamin B1 (1/1000) and GAPDH (1/1000) as nuclear and cytoplasmic markers respectively. Primary antibodies were detected with a horseradish peroxidase conjugated anti-rabbit IgG (1/5000).

4.1.2 TGF-β activation remains un-affected when cells are trypsinized and quickly processed

TGF-β is a cytokine well known to be involved in fibrosis. For this reason, this molecule is used to mimic the fibrotic condition. However, it was first necessary to determine if the trypsinization process affects TGF-β activation. To do this, MLE12 full lysates previously subjected to TGF-β treatment were analyzed in a WB. The main effectors of this signaling

pathway, the smad proteins, shown to be activated despite trypsinization in those cells that had been treated with TGF-β (**Figure 8**).

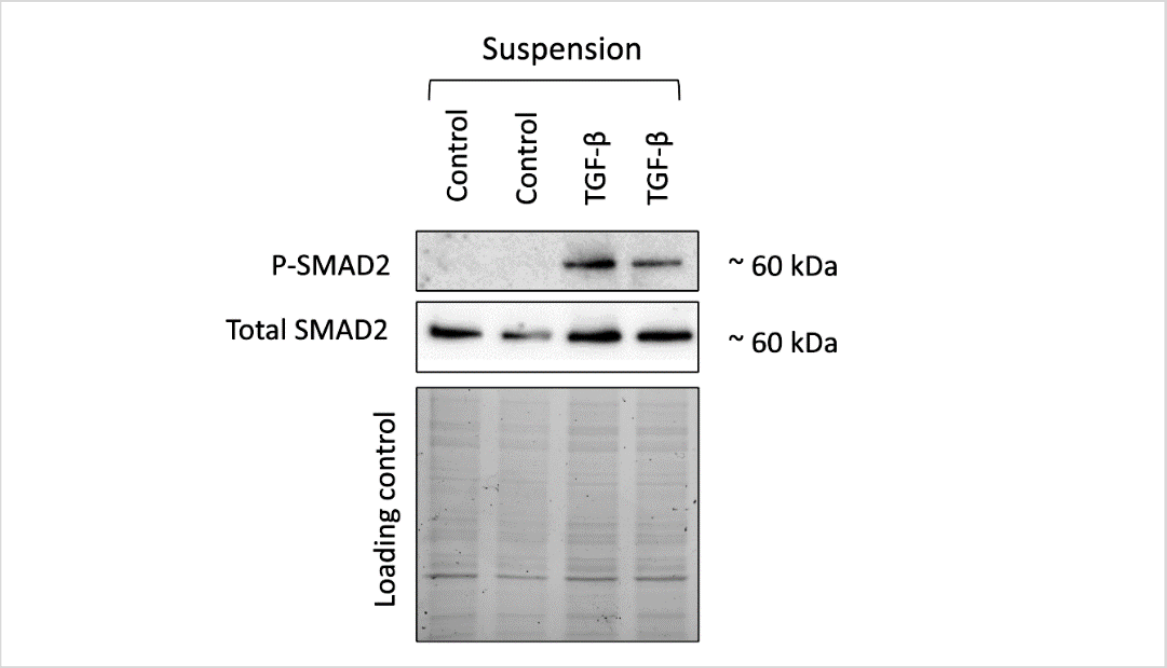

Figure 8. **Western blot analysis of smad proteins in trypsinized MLE12 cells after 4 hours 10 ng/mL TGF-β treatment.** Phosphorylated smad2 is only expressed in cells treated with TGF-β. Smad2 (1/500) and p-smad2 (1/500) antibodies were detected using a horseradish peroxidase conjugated anti-rabbit IgG (1/5000).

4.1.3 TGF-β causes a loss of YAP phosphorylated at serine 127 respect to total YAP

Since TGF- β is the main driver of fibrosis and YAP was found to be hyperactivated in IPF, it was expected to find a decrease in p-YAP in cells exposed to this growth factor. Therefore, a WB on trypsinized cells previously incubated with TGF-β was performed to evaluate the effect of TGF-β treatment on the effector proteins of the Hippo pathway. To do this, the expression of YAP phosphorylated at serine 127 was analyzed. The relevance of examining p-YAP (s127) levels lied in the fact that this phosphorylation prevents YAP nuclear localization and transcriptional activity (24). The resultant blot and its subsequent quantification reveal a loss of p-YAP (s127) in respect to total YAP protein in those cells that had received the treatment (**Figure 9**).

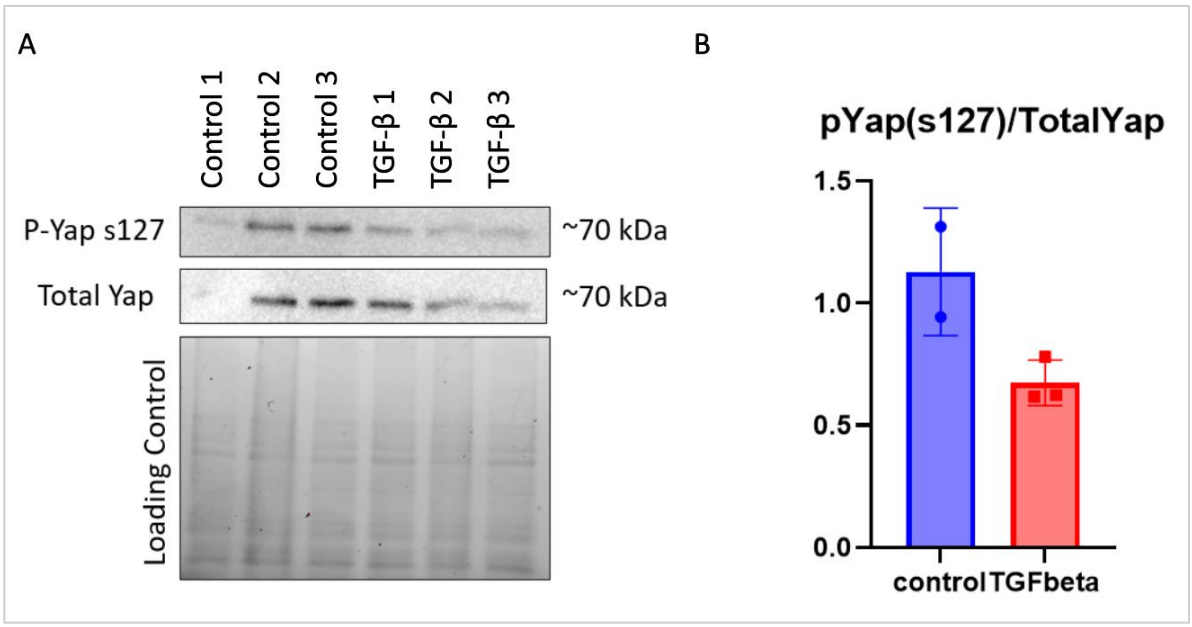

Figure 9. **Western blotting of decreased p-YAP (s127) expression in MLE12 cells treated with TGF-β and its quantification.** (A) YAP and p-YAP bands were detected using p-YAP s127 (1/500) followed by YAP (1/500) primary antibodies and revealed with a horseradish peroxidase conjugated anti-rabbit IgG (1/5000). Control 1 shows a weaker signal than the other control samples. (B) Bar graph showing a lower p-YAP (s127) to total YAP ratio in TGF-β treated cells. Control group (n=2), control 1 was discarded due to the weakness of the bands whereas all samples treated with TGF-β were used in the quantification (n=3).

4.1.4 Nuclear fraction is not detected in TGF-β treated MLE12 cells after subcellular fractionation

Even though there was a loss in p-YAP (s127) in cells subjected to TGF-β treatment, the exact localization of YAP still needed to be elucidated. To determine if YAP was entering the nucleus, we performed subcellular fractionation and then analyzed the presence of this protein in the nuclear fraction. The resultant blot was inconclusive due to the nuclear marker was not detected in MLE12 cells previously treated with TGF-β regardless of trypsinization (**Figure 10**). However, we also do not detect a cytoplasmic marker either. Therefore, although further discussion is needed to determine if nuclear proteins were not correctly separated from the ones in the cytoplasm or if the treatment applied negatively affects the detection of lamin B1 marker, our results indicate that the treated sample is molecularly different than the cytoplasmic fraction and that the lack of a lamin B1 is most likely due to the treatment and not the fractionation technique.

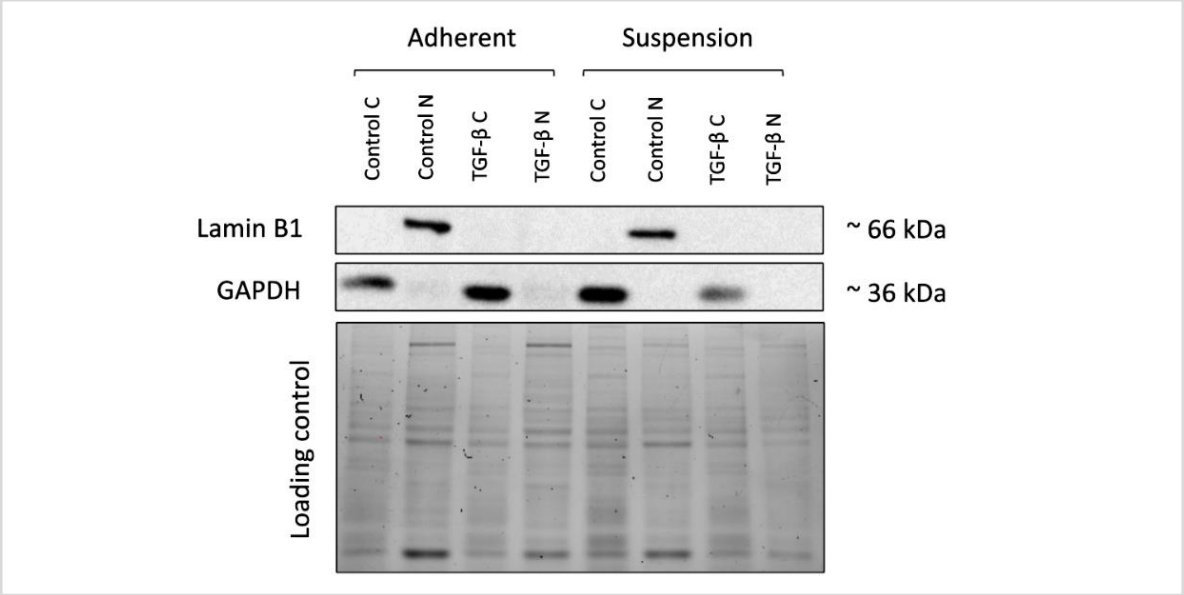

Figure 10. **Representative western blot of nuclear and cytoplasmic markers in MLE12 cells after TGF-β treatment followed by subcellular fractionation.** GAPDH was detected through all the samples while Lamin B1 was missing in TGF-β nuclear fractions. GAPDH and Lamin B1 antibodies concentration was 1/1000 and were detected using a horseradish peroxidase conjugated anti-rabbit IgG (1/5000). C= cytoplasmic fraction, N= nuclear fraction.

4.2 Optimization of immunoprecipitation protocol

As exposed in **Figure 6**, the main goal of these experiments is to identify which are the exact transcription factors that interact with Y/T. To accomplish the identification through proteomic analysis, it was first required to obtain the TFs-Y/T protein complexes. IP against Y/T was thought to be the most suitable technique for this purpose. However, the protocol needed to be optimized. IP optimization experiments were performed on leftover samples from subcellular fractionation as well as on protein lysates obtained by lysis of MLE12 cells employing RIPA buffer.

4.2.1 Y/T pulled down proteins are not detected in silver staining after elution with low pH commercial IgG elution buffer

The first protocol tested was which the manufacturer of protein A magnetic beads suggests. This protocol recommends a low pH commercial IgG elution buffer (pH 2.8) to elute obtained complexes from the beads. Moreover, we decided to add a preclearing prior step that consisted of incubating the magnetic beads with the antigen sample without adding antibodies. The resultant protein-bead complexes were discarded to ensure avoidance of non-specific binding.

Additionally, antibodies were diluted following the manufacturer's recommendations. In this case, Y/T was recommended at 1/50 for IP. The eluted samples from the IP experiment using these parameters were analyzed through SDS-PAGE followed by silver staining, a very sensitive technique for detecting small amounts of proteins in polyacrylamide gels. No immunoglobulin bands from Y/T pull down were detected in the resultant gel (**Figure 11A**). For that reason, the same experiment was repeated increasing the amount of antibodies used for the IP. The dilution ratio was decreased from 1/50 to 1/20. However, bands were still missing in Y/T wells (**Figure 11B**).

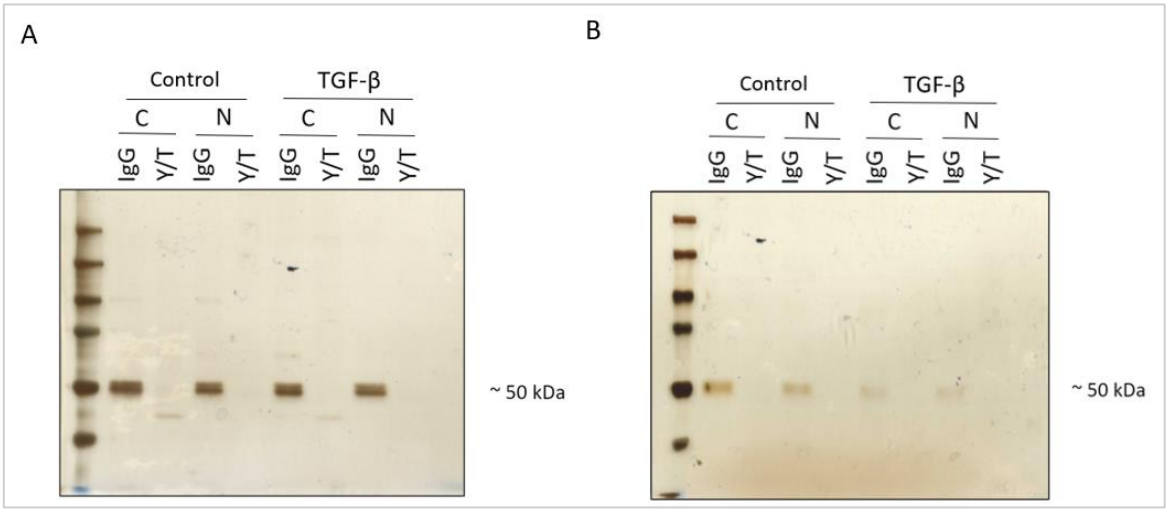

Figure 11. **Silver staining of pulled down proteins eluted with low pH commercial buffer.** Silver stained 10% polyacrylamide gel containing pulled down proteins from the resultant samples of subcellular fractionation experiments using Y/T or IgG isotype control antibodies at a concentration of 1/50 (A) or 1/20 (B) for the pull down. Bands of 50 kDa are observed in IgG wells whereas no identified proteins were found in Y/T wells. The amount of sample loaded was 32.6% of the elute and the staining was developed for 4 minutes. Ladder is shown in the first well (all blue from Bio Rad). C= cytoplasmic fraction N= nuclear fraction.

4.2.2 Y/T pulled down complexes eluted with alternative buffers are not detected by silver staining or western blot

In the interest of determining if the reason why proteins were not being detected after the IP process was related to the elution step, several different elution buffers were tested following the same protocol (**Figure 12**). SDS-PAGE reducing sample buffer was proposed to be a good alternative to directly run the resultant pull down in a polyacrylamide gel. Nonetheless, the protocol warned that it is not recommended to boil the sample if it contains rabbit antibodies, which was the case. Non-boiled samples eluted with this alternative buffer were analyzed through silver staining. The signal of the bands was noticeably weak due to a systematic error.

The sample was over-diluted, which decreased the amount of proteins loaded in the gel. However, some protein presence could still be detected. In fact, bands of ~63 kDa appeared in all conditions while 125 kDa bands were found only in IgG wells (**Figure 12A**). Then, the same experiment was performed increasing the volume of sample per well. Additionally, this time eluates were boiled at 95ºC for 5 minutes, which resulted in a stronger signal and a different band pattern, showing bands of ~50 kDa just in wells corresponding to IgG samples (**Figure 12B**). These samples were analyzed in WB as well, which resulted anew in the absence of signal from both YAP and TAZ. Immunoglobulins corresponding to Y/T antibodies were also not detected in the immunoblot (**Figure 12C**).

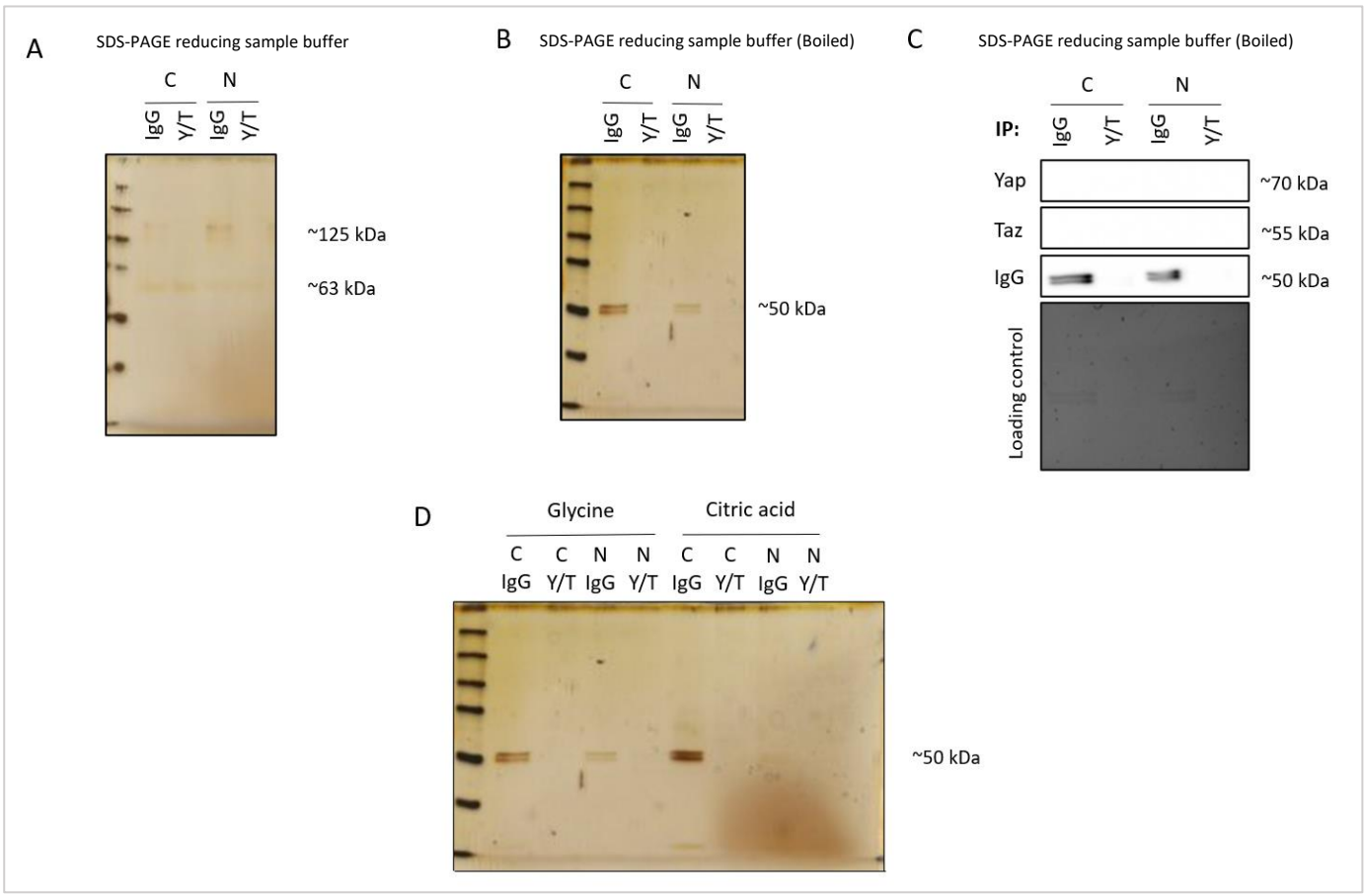

Figure 12. **Analysis of pulled down proteins using alternative elution buffers.** (A) Silver staining on pulled down samples eluted with SDS-PAGE reducing sample buffer without boiling. 63 and 125 kDa bands are observed. 125 kDa are just found in IgG wells. The amount of sample loaded was 7,5% of the eluate. (B) 9,25% of the proteins eluted with SDS-PAGE reducing sample buffer and boiled 5 min 95ºC in a silver stained gel. 50 kDa bands are detected in IgG samples. (C) western blot on samples from B. No signal was found for Y/T while IgG bands were detected in the control samples. The antibodies used were Y/T (1/500) and anti-rabbit IgG HRP conjugated (1/5000). (D) Silver stained gel containing the 65% of glycine and citric acid eluates. 50 kDa bands are observed in IgG wells. Silver staining was developed for 6 minutes. C= cytoplasmic fraction N= nuclear fraction.

To try more alternatives to elute the protein complexes from the magnetic beads, another experiment was designed. On this occasion, the selected elution buffers were either 100 mM glycine•HCl, pH 2.5-3.0 or 100 mM citric acid, pH 3.0, and the resultant samples were evaluated using silver staining. The same results as in the previous experiments were found, with bands of ~50 kDa just shown in IgG wells (**Figure 12D)**.

4.2.3 Y/T proteins do not bind randomly to protein A magnetic beads

To determine if Y/T proteins were being discarded in the preclearing, every resultant sample of each step of this process was analyzed in a WB. Additionally, protein A and protein G magnetic beads were compared to ensure there was not any problem related to the beads.

The experiment consisted of incubating the beads with the antigen sample without antibodies addition. After 20 minutes of incubation, beads were collected with a magnet and the leftover solution was named “collection 1”. The next step was to wash the beads with wash buffer and save that solution for analysis, this one was “collection 2”, after one more wash step called “collection 3”, proteins bound in a non-specific way to the beads were eluted using SDS-PAGE reducing sample buffer with boiling. This sample was named “beads eluate” (**Figure 13A**).

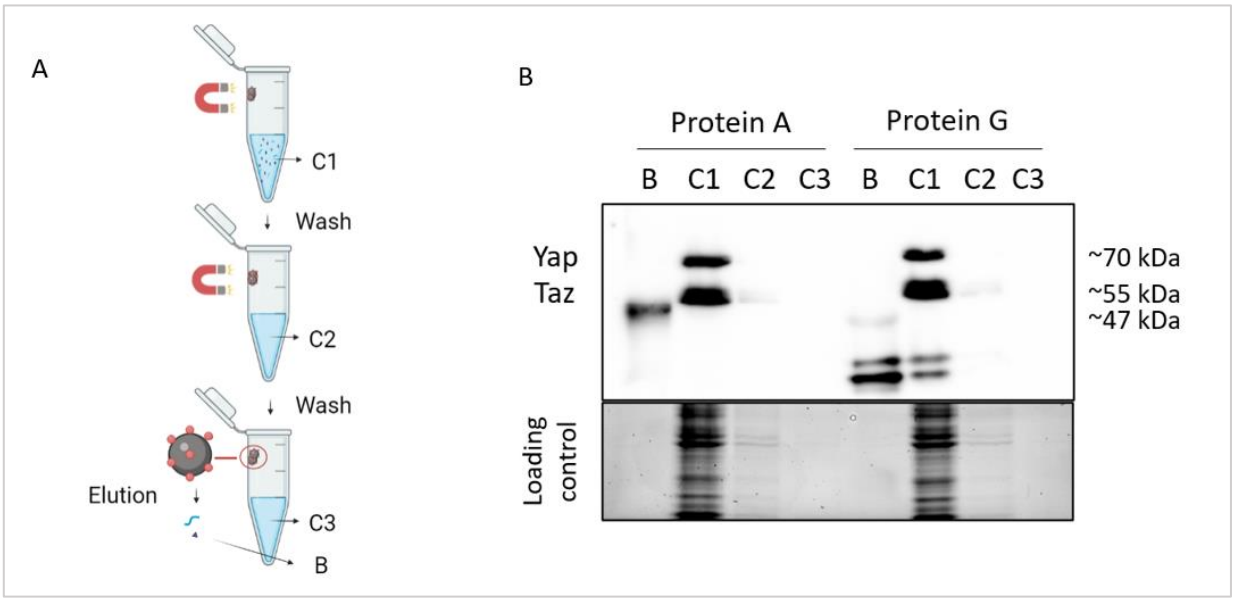

Figure 13. **Analysis of the preclearing step.** (A) Schematic representation of the samples obtention. (B) Western blot comparing non-specific binding of Y/T to protein A or protein G magnetic beads. Y/T are only detected in C1 using Y/T (1/500) and anti-rabbit IgG HRP conjugated (1/5000). C1= collection 1, C2= collection 2, C3= collection 3, B= beads eluate. Image created with Biorender.

Once all of them were collected, a WB against Y/T was performed. Both YAP and TAZ were detected in collection 1, while collections 2 and 3 did not show any signal. In contrast, a band of ~47 kDa corresponding to contaminating fragments of protein A was detected in the beads eluate sample (**Figure 13B**). These results confirm that Y/T were not randomly binding to protein A magnetic beads, so they are suitable to perform Y/T IP experiments.

4.2.4 Y/T are not detected after the immunoprecipitation of these proteins in the precleared sample using protein A magnetic beads

After demonstrating that Y/T were not randomly binding to protein A beads and they were in collection 1, the immunoprecipitation protocol eluting with the commercial low pH elution buffer was tested in the sample resulting from mixing collection 1, collection 2, and collection 3. Silver staining shown in **Figure 14A** exhibits the same pattern of bands in the Y/T pull down as the control. Nonetheless, a western blot was performed on these samples to elucidate if any of the bands corresponded to Y/T (**Figure 14B**).

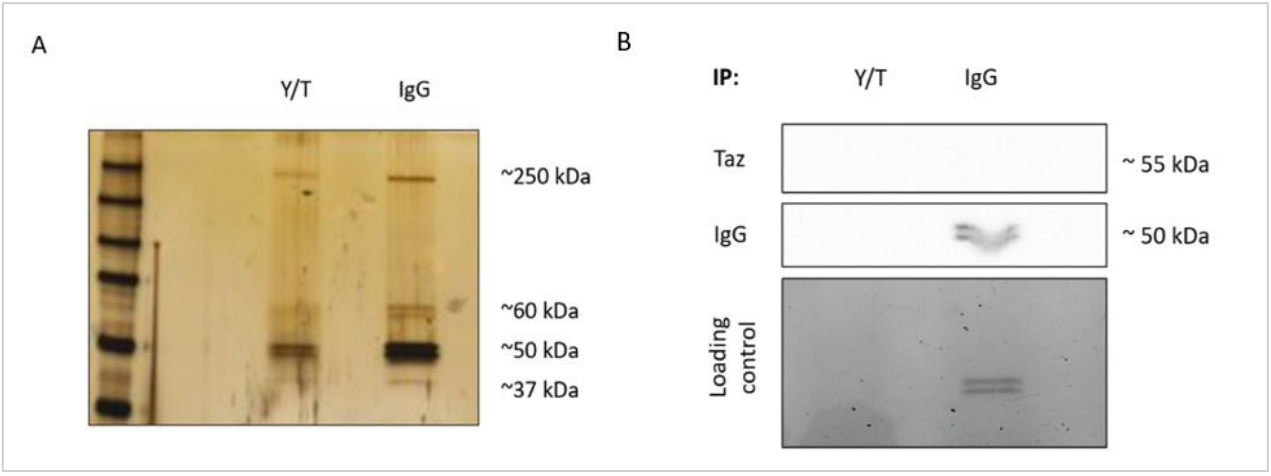

Figure 14. **Analysis of eluates after Y/T immunoprecipitation in precleared sample.** (A) Silver staining containing Y/T and control pulled down samples. The stain was developed for 7 minutes. (B) Western blotting of the same samples incubated with mouse Taz antibody (1/500) and detected with an anti-mouse IgG HRP conjugated (1/5000).

Despite using a mouse Taz antibody, the heavy chain of the IgG control was detected in the western blotting, revealing that this immunoglobulin showed cross-reactivity with other species. For this reason, other rabbit IgG isotype control was used in all the experiments performed thereafter.

4.2.5 Y/T proteins are not present in the flowthrough of the immunoprecipitation performed in the precleared sample

On account of Y/T were not detected after the elution of the beads, we wanted to elucidate if these proteins were in the flowthrough obtained after separating the complex formed by the beads and the antibodies bound to the specific protein they recognize from the rest of the antigen sample (**Figure 15A**). However, western blotting on the resultant flowthrough showed no presence of Y/T in this sample (**Figure 15B**).

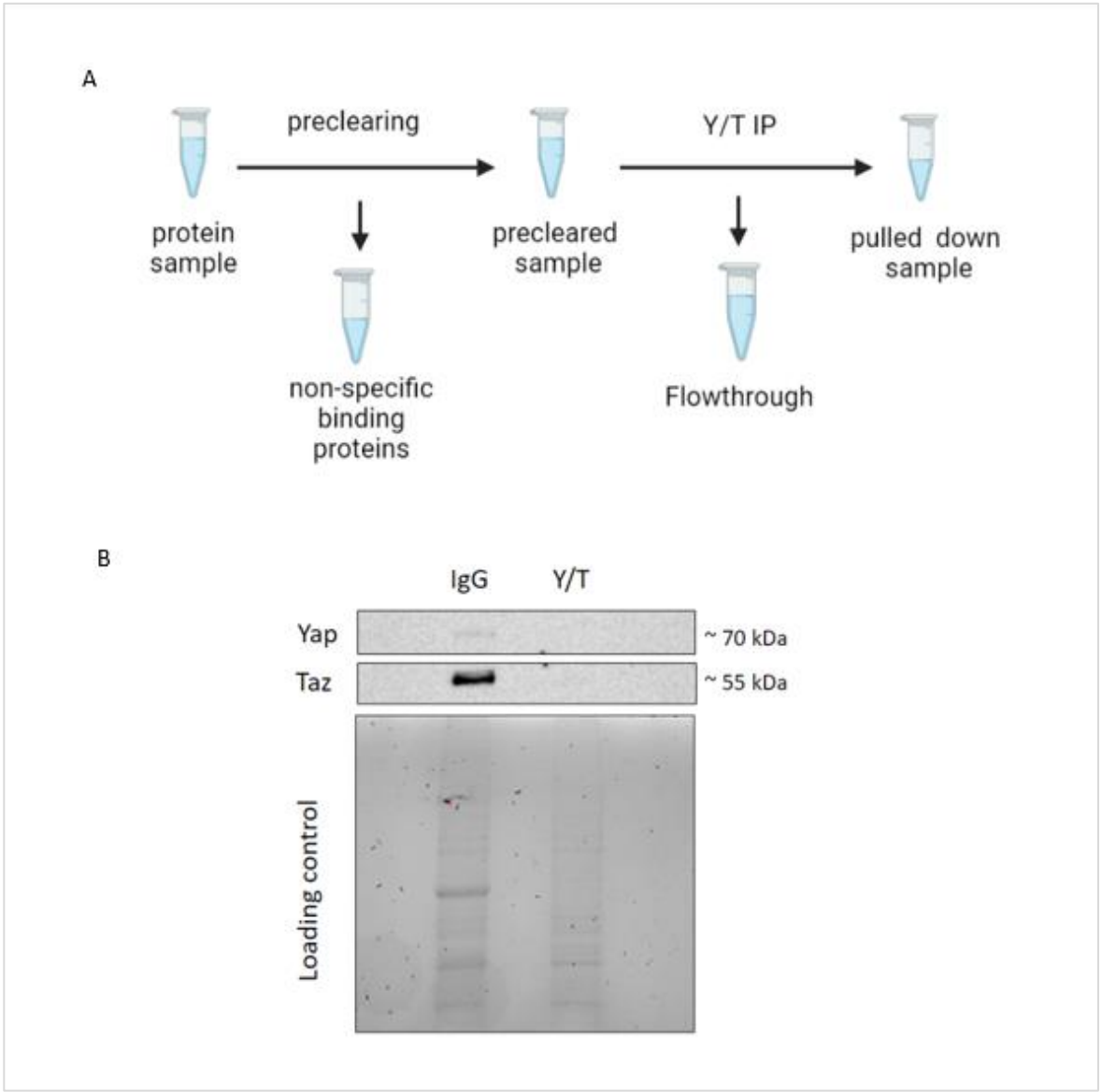

Figure 15. **Western blot on flowthrough samples for Y/T presence analysis.** (A) Schematic diagram of the process by which flowthrough is produced. (B) Immunoblot showing Y/T proteins only in the control sample´s flowthrough. Antibodies used: Y/T (1/500), anti-specie IgG HRP conjugated (1/5000). Created with Biorender.

4.2.6 Proteins are correctly eluted from the protein A magnetic beads

The absence of Y/T proteins in the analyzed samples encouraged the need to elucidate whether the antibodies were still bound to the magnetic beads after the elution step. To do this, an immunofluorescence experiment was performed. The approach consisted of incubating the beads (control negative), the complex formed by the beads bound antibody and the specific protein they recognize (control positive), and the beads after the elution step (sample of interest) with a goat anti-rabbit IgG Alexa fluor 568 conjugated antibody (**Figure 16**).

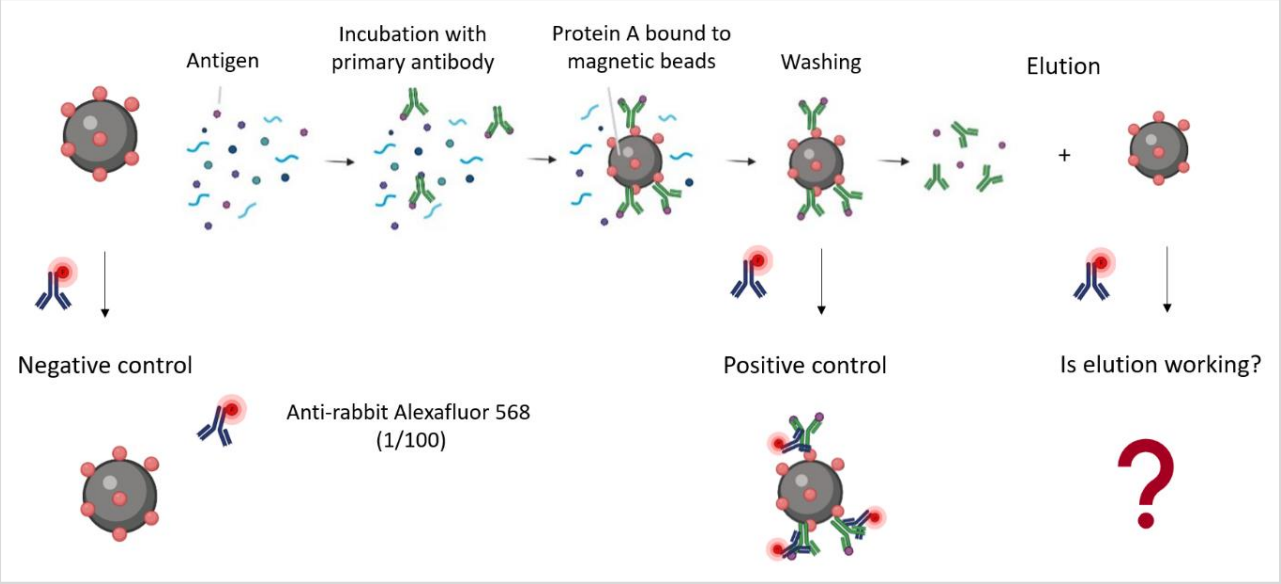

Figure 16. **Schematic diagram of the immunofluorescence experiment to analyze if the proteins are eluted from the beads.** Proteins were eluted from the beads using low pH commercial IgG elution buffer (pH 2.8). Diagram created using Biorender.

The resultant images showed no fluorescence in the beads after elution, which confirmed that samples containing IgG control antibody showed an excess of the fluorescent signal as well as aggregates in positive control brightfield images, suggesting that the amount of antibody used was considerably higher than the Y/T one (**Figure 17**).

As a result of the differences between IgG and Y/T antibodies detected in the immunofluorescence and brightfield images, the stock concentration of both immunoglobulins was revised ascertaining the inequality. While Y/T was 0,031 µg/µl, the new IgG came at a considerably higher concentration (1.675 µg/µl) as well as the one that showed cross-reactivity with other species (0,91 µg/µl). Thus, all the previous experiments had been affected by this mistake regardless of the IgG used.

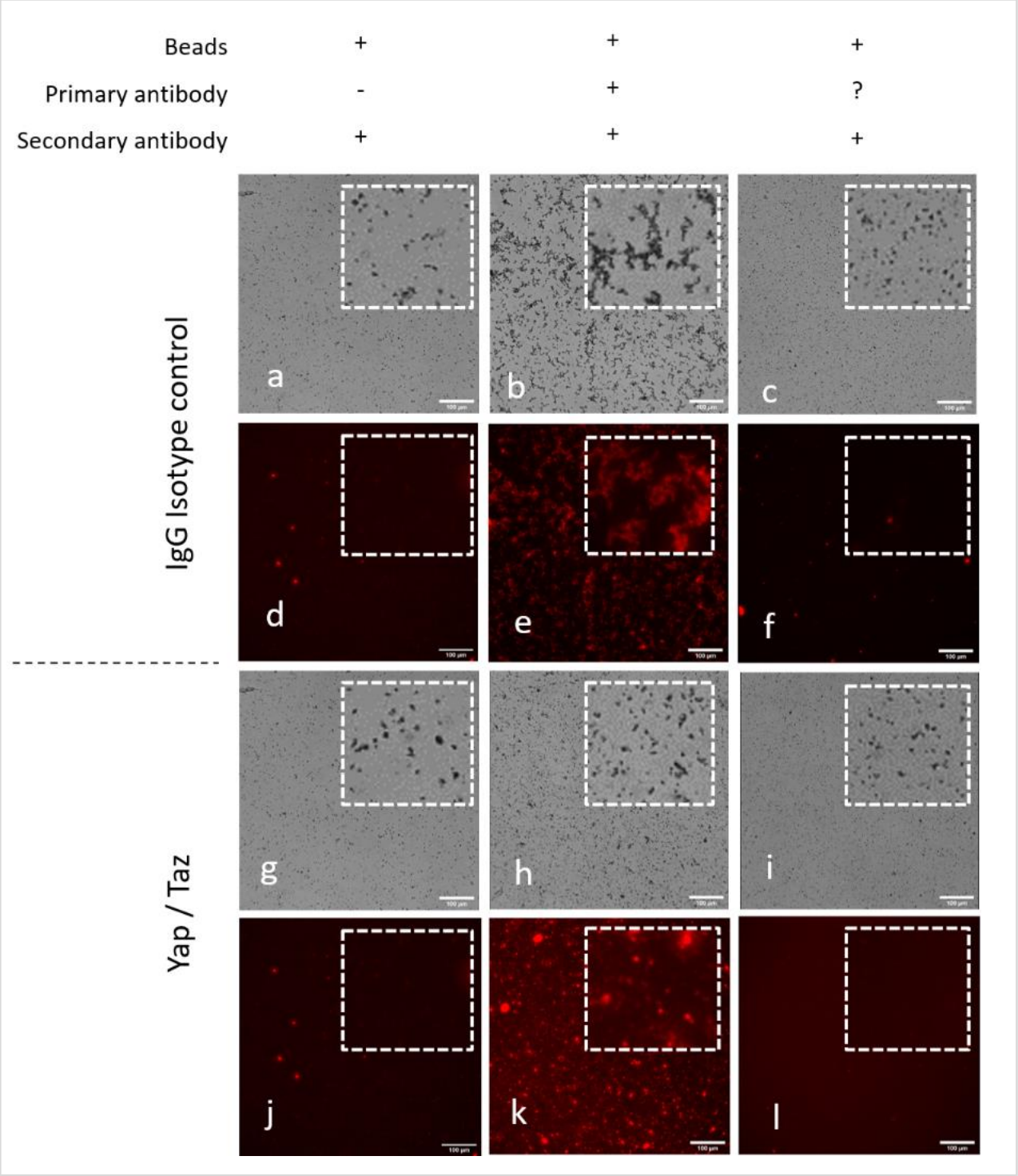

Figure 17. Corresponding immunofluorescence and bright-field microscopy images showing a goat anti-rabbit IgG Alexa Fluor 568 conjugated antibody (1/100) incubated with protein A magnetic beads (a,d,g,j), the immunoprecipitation complex formed by the beads bound to IgG isotype control (b,e) or Y/T (h,k) antibodies, and with beads obtained after the elution of the IgG control (c,f) or Y/T immunoglobulin (i,l). Question mark refers to whether the antibody remains on the beads after elution or not. All micrographs were taken under identical exposure time with a 20X objective. Insets exhibit 5X magnification. Scale bar=100µm.

4.2.7 The equality in the concentration of Y/T and IgG antibodies resulted in the detection of Y/T pulled down complexes

To determine if the disparity in the antibody´s concentration was the reason why samples containing Y/T antibodies were not detected, the same immunofluorescence experiment was performed.

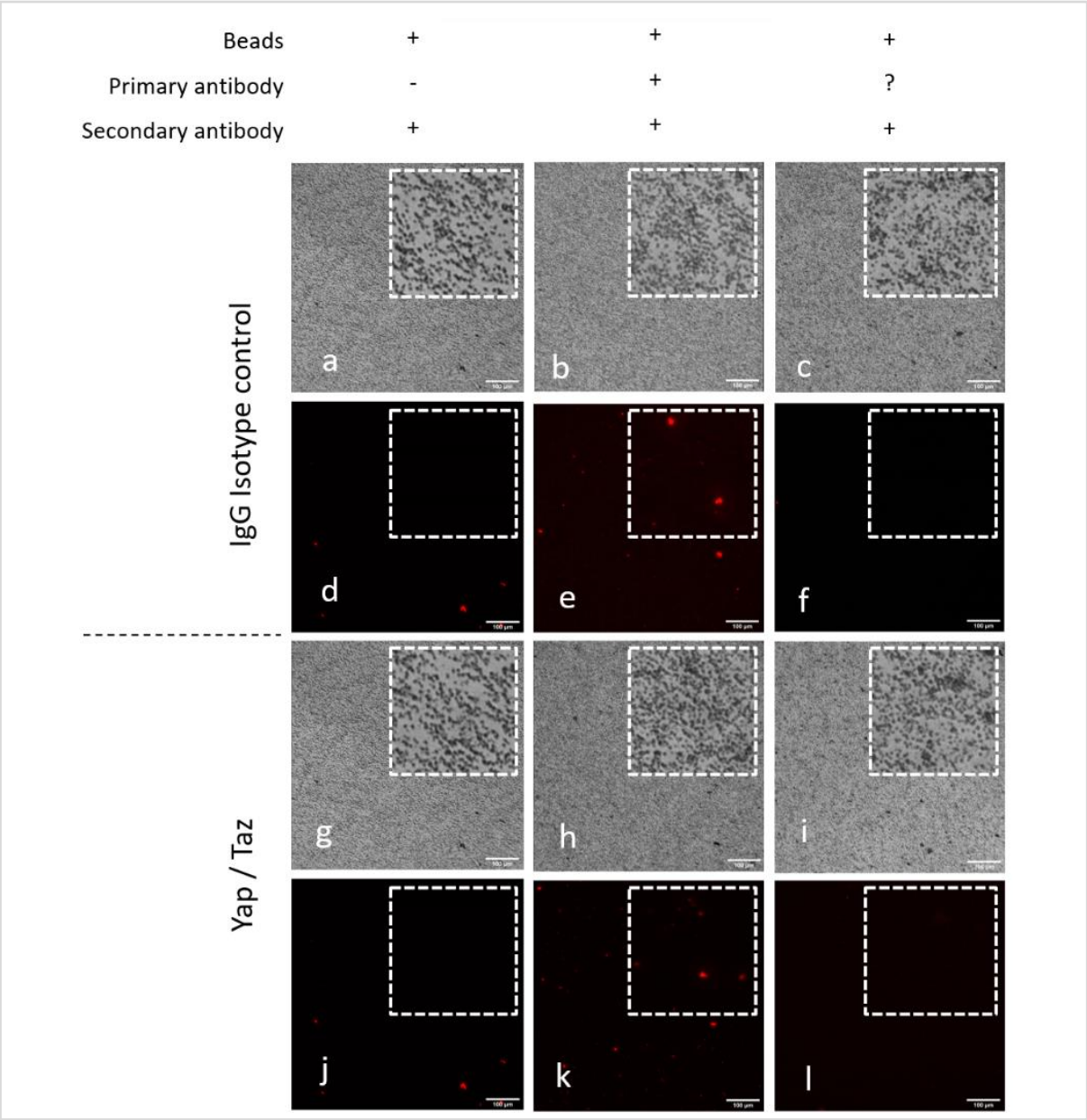

Figure 18. Immunofluorescence and bright-field microscopy images showing a goat anti-rabbit IgG Alexa Fluor 568 conjugated antibody (1/100) incubated with only beads (a,d,g,j), beads bound to IgG isotype control (b,e) or Y/T (h,k) antibodies, and beads after the elution of IgG (c,f) or Y/T (i,l) immunoglobulins. Question mark refers to whether the antibody remains on the beads after elution or not . All images were taken under identical exposure time using a 20X objective. Insets exhibit 5X magnification. Scale bar=100µm.

This time, IgG concentration was adjusted to ensure that the amount of Y/T and IgG isotype control antibodies used for the IP was the same (0,062 µg). Immunofluorescence images show that the antibody amounts were correctly adjusted as well as corroborate that proteins are separated from the beads after elution (**Figure 18**).

In addition, proteins eluted from the beads using the low pH commercial buffer were analyzed through silver staining and WB. As a consequence of the decrease in IgG antibody concentration, bands corresponding to Y/T pulled down complexes were detected in the silver staining showing a different pattern compared to the IgG control sample, confirming the binding specificity of Y/T antibody (**Figure 19**). However, no bands were distinguished in the western blot (results not shown).

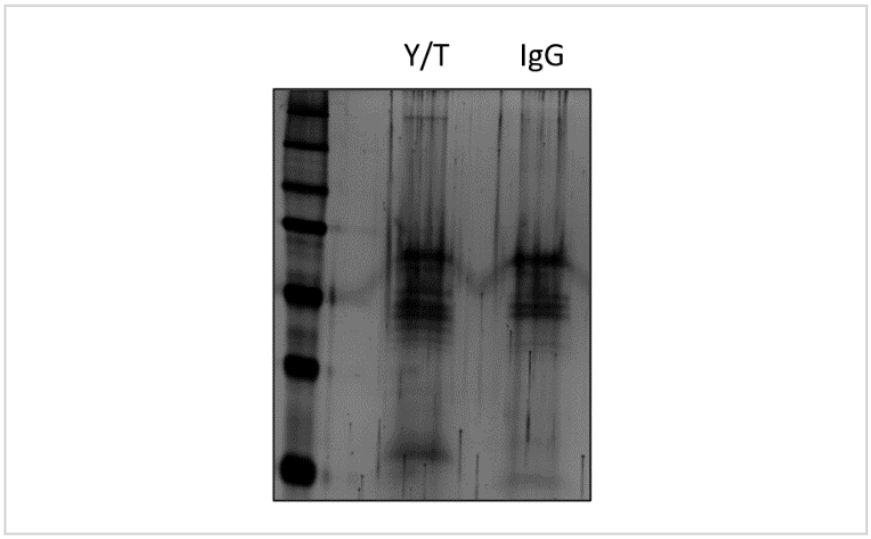

Figure 19. **Y/T-TFs complexes are isolated from full lysates after immunoprecipitation protocol.** (A) Silver-stained gel developed for 7 minutes showing different bands pattern in Y/T pull down compared to the control. First lane corresponds to all blue prestained protein ladder (10-250 kD) from BioRad.

5. DISCUSSION

IPF is a chronic and progressive interstitial lung disease with a survival rate of 2-5 years after diagnosis. Although genetic susceptibility, as well as several environmental risk factors, have correlated with this disease, the exact causes remain unclear. In recent years, two antifibrotic agents, nintedanib and pirfenidone, have been approved by the FDA as the pharmacological treatment of IPF, but these drugs can only reduce rates of disease progression. In fact, other than lung transplantation, no treatment has shown reversal of alveolar damage caused by fibrosis. However, new effective therapies to increase the survival of these patients are desperately needed due to long transplant waiting lists, lack of compatible donors, and complications derived from surgeries. Different pathways involved in development such as Notch, Wnt, or Hippo have been shown to be reactivated during IPF. Moreover, unpublished data from Darcy´s Wagner group demonstrate an increased nuclear localization of Y/T not only in fibroblasts but also in distal epithelial cells. Since the major roles of Hippo signaling pathway are organ size control during development and regeneration, it is reasonable to think that tissue damage is so severe that the cellular machinery tries to reactivate developmental pathways in an insufficient attempt to achieve normal lung architecture (25). Therefore, it is essential to distinguish which Y/T binding TFs favour the fibrotic condition to develop novel therapies which only target interactions that promote the disease. In this study, we validate subcellular fractionation as well as optimize an IP protocol using conditions compatible with MS proteomics for the subsequent identification of Y/T binding partners using this technique.

Mice cells are suspended for in vivo work, so we wanted to mimic this scenario. For this purpose, adherent and suspended MLE12 were used in the experiments carried out to demonstrate the effectiveness of the subcellular fractionation protocol. In addition to this, it was interesting to test the protocols in suspended cells since studies such as the one accomplished by Zhao *et al*. show that cell detachment activates the Hippo pathway via cytoskeleton reorganization, meaning that Y/T become phosphorylated and retained in the cytoplasm (26). This is relevant because during fibrosis Y/T are hyperactivated, thus, suspending cells can help in the comparison between control MLE12 and those treated with a profibrotic agent. WB performed in both adherent and trypsinized cells confirm that the subcellular fractionation protocol works effectively in both conditions. Interestingly, BCA assay after subcellular fractionation showed no differences in the total number of proteins obtained from both conditions, while the nuclear fraction relative to the cytoplasmic one in suspended cells was found to be noticeably higher. Although this finding was unexpected and further

research is needed to elucidate its rationale, it suggests that the subcellular fractionation protocol is more effective in previously suspended cells.

TGF-β is a cytokine involved in the development of fibrosis in diverse organs, reason why it is commonly used to mimic the fibrotic condition in vitro (27–29). In this project, we demonstrate that TGF-β activation remains un-affected when cells are trypsinized. In addition to this, many studies exhibit that there is clear crosstalk between TGF-β and Hippo pathway. In fact, some of them show in their work that TGF-β promotes Y/T activation (30,31). As this had not been shown in lung epithelial cells, we tested the effect of TGF-β treatment in MLE12 cell line and found a loss of p-Yap (s127) relative to total Yap (**Figure 9**). This finding confirms that Yap phosphorylation is not affected by trypsinization and, in line with results observed in studies conducted in other cell types, indicates that Yap could be active in TGF-β treated MLE12 cells even after trypsinization. However, this information was not enough to confirm that Yap enters the nucleus. Therefore, we performed subcellular fractionation following TGF-β treatment to determine the exact localization of Yap. Unexpectedly, the nuclear marker in treated cells was not detected in western blot experiments. Similarly to our results, the study by Comaills *et al.* observes that TGF-β induces genomic instability by suppressing multiple nuclear envelope proteins, such as lamin B1, which could explain our data as the nuclear marker is consistently detected in non-TGF-β-treated cells as well as the cytoplasmic marker is not detected in any nuclear fraction (32). Additionally, since the cytoplasmic marker was not detected in those fractions either, our results indicate that the non-detection of a lamin B1 is most likely due to the treatment. In support of this, immunofluorescence experiments from Darcy Wagner´s group show increased nuclear localization of Y/T after 1ng/mL TGF-β treatment in MLE12 cells (unpublished data). Nonetheless, another nuclear marker needs to be tested to validate subcellular fractionation on these samples.

IP is a widely extended technique for the enrichment of low-abundant protein targets prior to MS analysis. However, different aspects of the process such as the use of particular types of beads, non-specific bindings, and the use of detergents, viscous or high-salt solutions in wash and elution buffers, lead to incompatibility with MS. To avoid this, we used protein A magnetic beads and MS-compatible reagents to immunoprecipitate Y/T following the manufacturer´s protocol. According to our results, proteins do not randomly bind to the surface of protein A magnetic beads, which makes them suitable for Y/T IP. This was critical as their magnetic properties allowed for rapid processing of the samples and enabled them to be analyzed by MS without causing incompatibility problems.

Utilizing an appropriate amount of antibodies is essential to successfully immunoprecipitate proteins. Even though the Y/T antibody was advised to be used at a dilution rate of 1/50 for IP in its datasheet, the amount of Y/T added following this recommendation (0,062 µg) was considerably lower than the minimum required by the IP protocol (5 µg). However, Yuan *et al*. evidence that the IP protocol works effectively even using 0,014 µg of antibody, so we assumed that the amount employed in our experiments is sufficient for Y/T pull down (33). On the other hand, not only is important to know the stock antibody concentration to be aware of the exact amount used in each experiment but also is crucial to adjust it so that there is an equivalence between IgG control and specific antibodies. In fact, our immunofluorescence results emphasise the relevance of this by evidencing the successful elution of proteins from the beads, meaning that even though Y/T complexes were being immunoprecipitated and correctly eluted, the disparity in the amount of IgG and Y/T antibodies interfered in the detection of bands in Y/T pulled down samples due to the strong signal of the isotype control. In support of this, we did not find Y/T in the preclearing and flowthrough samples corresponding to the Y/T pull down, while they were detected in the flowthrough of the control samples. Accordingly, adjusting the concentration of the different antibodies resulted in the appearance of bands in the Y/T sample in silver staining. Moreover, Y/T pull down in this gel showed a different pattern compared to the control, thus demonstrating the effectiveness of the IP protocol. However, WB on these samples showed no bands. A possible explanation for this could be that the amount of protein might be too low to be detected using this technique.

As a future perspective, Y/T complexes eluted from the beads could be analyzed using MS, which is highly sensitive and could identify Y/T even though they are not detected in WB. Antibodies used for the IP and WB are the same, therefore, identical antigen is recognized in both experiments. As how proteins are cleared from the beads remains unknown, it is possible that Y/T have suffered modifications due to their binding to IP antibodies, which could explain the lack of bands in WB after the pull down. Since we have only tried low pH elution buffers, it could also be interesting to try other MS-compatible buffers working with high pH, ionic strength, or denaturing conditions. Additionally, an IP experiment using different concentrations of antibody could be carried out to determine whether the detection of bands in a WB is directly proportional to the amount of antibody, as well as to elucidate the minimum amount of Y/T antibody needed to obtain the best results.

Finally, on account of our final goal is to compare the TFs that Y/T bind to in the fibrotic and healthy condition, it is necessary to find an alternative nuclear marker which is not affected by TGF-β treatment to validate subcellular fractionation in samples mimicking fibrosis. In their

work, Guard *et al.* propose the nuclear matrix protein p84 as a good nuclear marker to verify the purity of nuclear extracts in subcellular fractionation assays (34). Once this is optimized, subcellular fractionation would be performed in control and TGF-β-treated cells followed by Y/T IP for the subsequent MS analysis. These results would provide valuable information to verify the data obtained through state-of-the-art bioinformatics tools.

6. CONCLUSIONS

This thesis project aimed to optimize an MS-compatible immunoprecipitation protocol for pulling down Y/T proteins after subcellular fractionation of murine alveolar epithelial cells to identify Y/T-interacting TFs in the context of IPF. Taking this into account, the main conclusions of this work are:

- Although subcellular fractionation protocol effectively separates cytoplasmic from nuclear fraction in MLE12 cells, a good nuclear marker is needed to do analysis of experiments such as the TGF-β treatment. However, the protocol seems to separate fractions well enough to move further for experiments like MS where an individual marker isn't needed.

- TGF-β activation remains un-affected when cells are trypsinized and quickly processed and the treatment with this cytokine causes a loss of YAP phosphorylated at serine 127 respect to total YAP, confirming that Yap phosphorylation is not affected by trypsinization as well as indicating that Yap could be active in TGF-β treated MLE12 cells even after trypsinization.

- Protein A magnetic beads are suitable for Y/T immunoprecipitation due to proteins do not randomly bind to their surface.

- Proteins are correctly eluted from the beads using low pH elution buffers.

- Y/T complexes are successfully isolated from full lysates after immunoprecipitation protocol using 0,062 µg of antibody. However, further research is needed to determine if a higher antibody concentration enables Y/T detection in western blotting after the pull down.

7. BIBLIOGRAPHY

1. Vinay Kumar, Abul K. Abbas, Jon C. Aster. Robbins. Patología humana. 10a ed. España: Elsevier; 2018. 495–508 p.
2. Richeldi L, Collard HR, Jones MG. Idiopathic pulmonary fibrosis. The Lancet. 2017 May 13;389(10082):1941–52.
3. Martinez FJ, Collard HR, Pardo A, Raghu G, Richeldi L, Selman M, et al. Idiopathic pulmonary fibrosis. Nat Rev Dis Primers [Internet]. 2017 Oct 20 [cited 2021 Nov 29];3. Available from: https://pubmed.ncbi.nlm.nih.gov/29052582/
4. King TE, Pardo A, Selman M. Idiopathic pulmonary fibrosis. The Lancet. 2011;378(9807):1949–61.
5. Lederer DJ, Martinez FJ. Idiopathic Pulmonary Fibrosis. Longo DL, editor. New England Journal of Medicine [Internet]. 2018 May 10 [cited 2021 Nov 29];378(19):1811–23. Available from: http://www.nejm.org/doi/10.1056/NEJMra1705751
6. Ley B, Collard HR. Epidemiology of idiopathic pulmonary fibrosis. Clinical Epidemiology [Internet]. 2013 Nov 25 [cited 2021 Nov 29];5(1):483. Available from: /pmc/articles/PMC3848422/
7. Kia'i N, Bajaj T. Histology, Respiratory Epithelium. StatPearls [Internet]. 2021 May 10 [cited 2021 Nov 29]; Available from: https://www.ncbi.nlm.nih.gov/books/NBK541061/
8. Sepílveda J SA. Sistema respiratorio | Texto Atlas de Histología. Biología celular y tisular, 2e [Internet]. McGraw Hill. 2014 [cited 2021 Nov 29]. Available from: https://accessmedicina.mhmedical.com/content.aspx?bookid=1506&sectionid=98183423
9. Barkauskas CE, Chung MI, Fioret B, Gao X, Katsura H, Hogan BLM. Lung organoids: Current uses and future promise. Development (Cambridge). 2017 Mar 15;144(6):986–97.
10. Barkauskas CE, Cronce MJ, Rackley CR, Bowie EJ, Keene DR, Stripp BR, et al. Type 2 alveolar cells are stem cells in adult lung. The Journal of Clinical Investigation [Internet]. 2013 Jul 1 [cited 2021 Nov 29];123(7):3025. Available from: /pmc/articles/PMC3696553/
11. Wu H, Yu Y, Huang H, Hu Y, Fu S, Wang Z, et al. Progressive Pulmonary Fibrosis Is Caused by Elevated Mechanical Tension on Alveolar Stem Cells. Cell [Internet]. 2020 Jan 9 [cited 2021 Nov 30];180(1):107-121.e17. Available from: http://www.cell.com/article/S009286741931284X/fulltext
12. Wang ZN, Tang XX. New Perspectives on the Aberrant Alveolar Repair of Idiopathic Pulmonary Fibrosis. Frontiers in Cell and Developmental Biology. 2020 Sep 30;8:1045.
13. Jiang P, Rubio RG de, Hrycaj SM, Gurczynski SJ, Riemondy KA, Moore BB, et al. Ineffectual Type 2 to Type 1 Alveolar Epithelial Cell Differentiation in Idiopathic

Pulmonary Fibrosis: Persistence of the KRT8hi Transitional State. American Journal of Respiratory and Critical Care Medicine [Internet]. 2020 Jun 1 [cited 2021 Nov 30];201(11):1443–7. Available from: /pmc/articles/PMC7258651/

14. Riemondy KA, Jansing NL, Jiang P, Redente EF, Gillen AE, Fu R, et al. Single-cell RNA sequencing identifies TGF-β as a key regenerative cue following LPS-induced lung injury. JCI Insight. 2019;4(8).

15. Piersma B, Bank RA, Boersema M. Signaling in fibrosis: TGF-β, WNT, and YAP/TAZ converge. Frontiers in Medicine. 2015;2(SEP):59.

16. Selman M, López-Otín C, Pardo A. Age-driven developmental drift in the pathogenesis of idiopathic pulmonary fibrosis. European Respiratory Journal [Internet]. 2016 [cited 2021 Dec 1]; Available from: http://ow.ly/LN5W300wHOj

17. Hansen CG, Moroishi T, Guan KL. YAP and TAZ: A nexus for Hippo signaling and beyond. Vol. 25, Trends in Cell Biology. Elsevier Ltd; 2015. p. 499–513.

18. Plouffe SW, Lin KC, Moore JL, Tan FE, Ma S, Ye Z, et al. The Hippo pathway effector proteins YAP and TAZ have both distinct and overlapping functions in the cell. The Journal of Biological Chemistry [Internet]. 2018 Jul 13 [cited 2021 Dec 2];293(28):11230. Available from: /pmc/articles/PMC6052207/

19. Barry ER, Camargo FD. The Hippo superhighway: Signaling crossroads converging on the Hippo/Yap pathway in stem cells and development. Vol. 25, Current Opinion in Cell Biology. Elsevier Ltd; 2013. p. 247–53.

20. Meng Z, Moroishi T, Guan KL. Mechanisms of Hippo pathway regulation. Genes & Development [Internet]. 2016 Jan 1 [cited 2021 Dec 4];30(1):1. Available from: /pmc/articles/PMC4701972/

21. Zheng Y, Pan D. The Hippo Signaling Pathway in Development and Disease. Cell press [Internet]. 2019 [cited 2021 Dec 4]; Available from: https://doi.org/10.1016/j.devcel.2019.06.003

22. Panciera T, Azzolin L, Cordenonsi M, Piccolo S. Mechanobiology of YAP and TAZ in physiology and disease. Vol. 18, Nature Reviews Molecular Cell Biology. Nature Publishing Group; 2017. p. 758–70.

23. Liu F, Lagares D, Choi KM, Stopfer L, Marinković A, Vrbanac V, et al. Translational Research in Acute Lung Injury and Pulmonary Fibrosis: Mechanosignaling through YAP and TAZ drives fibroblast activation and fibrosis. American Journal of Physiology - Lung Cellular and Molecular Physiology [Internet]. 2015 Feb 2 [cited 2022 Jun 15];308(4):L344. Available from: /pmc/articles/PMC4329470/

24. Moon S, Kim W, Kim S, Kim Y, Song Y, Bilousov O, et al. Phosphorylation by NLK inhibits YAP-14-3-3-interactions and induces its nuclear localization. EMBO Reports [Internet]. 2017 Jan [cited 2022 May 4];18(1):61. Available from: /pmc/articles/PMC5210122/

25. Chanda D, Otoupalova E, Smith SR, Volckaert T, de Langhe SP, Thannickal VJ. Developmental Pathways in the Pathogenesis of Lung Fibrosis. Mol Aspects Med

[Internet]. 2019 Feb 1 [cited 2022 Jun 4];65:56. Available from: /pmc/articles/PMC6374163/

26. Zhao B, Li L, Wang L, Wang CY, Yu J, Guan KL. Cell detachment activates the Hippo pathway via cytoskeleton reorganization to induce anoikis. Genes Dev [Internet]. 2012 Jan 1 [cited 2022 Jun 4];26(1):54–68. Available from: https://pubmed.ncbi.nlm.nih.gov/22215811/

27. Fernandez IE, Eickelberg O. The impact of TGF-β on lung fibrosis: from targeting to biomarkers. Proc Am Thorac Soc [Internet]. 2012 Jul 15 [cited 2022 Jun 5];9(3):111–6. Available from: https://pubmed.ncbi.nlm.nih.gov/22802283/

28. Denton CP, Ong VH, Xu S, Chen-Harris H, Modrusan Z, Lafyatis R, et al. Therapeutic interleukin-6 blockade reverses transforming growth factor-beta pathway activation in dermal fibroblasts: insights from the faSScinate clinical trial in systemic sclerosis. Annals of the Rheumatic Diseases [Internet]. 2018 Sep 1 [cited 2022 Jun 5];77(9):1362. Available from: /pmc/articles/PMC6104680/

29. Hinz B. Mechanical aspects of lung fibrosis: a spotlight on the myofibroblast. Proc Am Thorac Soc [Internet]. 2012 Jul 15 [cited 2022 Jun 5];9(3):137–47. Available from: https://pubmed.ncbi.nlm.nih.gov/22802288/

30. Nakamura R, Hiwatashi N, Bing R, Doyle CP, Branski RC. Concurrent YAP/TAZ and SMAD signaling mediate vocal fold fibrosis. Scientific Reports |. 123AD;11:13484.

31. Szeto SG, Narimatsu M, Lu M, He X, Sidiqi AM, Tolosa MF, et al. YAP/TAZ Are Mechanoregulators of TGF- β-Smad Signaling and Renal Fibrogenesis. J Am Soc Nephrol [Internet]. 2016 [cited 2022 Jun 5];27(10):3117–28. Available from: https://pubmed.ncbi.nlm.nih.gov/26961347/

32. Comaills V, Kabeche L, Morris R, Zou L, Haber DA, Correspondence SM. Genomic Instability Is Induced by Persistent Proliferation of Cells Undergoing Epithelial-to-Mesenchymal Transition Accession Numbers GSE89152. CellReports [Internet]. 2016 [cited 2022 Jun 5];17:2632–47. Available from: http://dx.doi.org/10.1016/j.celrep.2016.11.022

33. Yuan Y, Park J, Feng A, Awasthi P, Wang Z, Chen Q, et al. YAP1/TAZ-TEAD transcriptional networks maintain skin homeostasis by regulating cell proliferation and limiting KLF4 activity. Nature Communications 2020 11:1 [Internet]. 2020 Mar 19 [cited 2022 Jun 13];11(1):1–14. Available from: https://www.nature.com/articles/s41467-020-15301-0

34. Guard SE, Ebmeier CC, Old WM. Label-Free Immunoprecipitation Mass Spectrometry Workflow for Large-scale Nuclear Interactome Profiling. JoVE (Journal of Visualized Experiments) [Internet]. 2019 Nov 17 [cited 2022 Jun 13];2019(153):e60432. Available from: https://www.jove.com/v/60432/label-free-immunoprecipitation-mass-spectrometry-workflow-for-large

8. SUPPLEMENTARY INFORMATION

Table S1. **Stain free Tris-HCl 1,5mm 10% gels recipe**. Indicated volumes are calculated for 2,5 gels. The mixture should start with the addition of the highest volumes while TEMED should be the last one. The resolver gel is first polymerized, once it becomes solid, stacking gel solution is added to the cast and the appropriate comb is chosen to form the desired number of wells.

Stain free Tris-HCl 1,5mm 10% gels		
Quantities for 2,5 gels	**Stacking (mL)**	**Resolver (mL)**
40% acrylamide (37,5:1)	0,938	5
dH2O	4,905	10,48
0,5 M Tris pH6,8	1,5	-
1,5 M Tris pH 8,8	-	4
10% SDS	0,075	0,2
10% APS	0,075	0,2
TEMED	0,008	0,02
2,2,2, Trichloroethanol	-	0,1